Report

Cell Reports

MicroRNA-9 Couples Brain Neurogenesis and Angiogenesis

Graphical Abstract

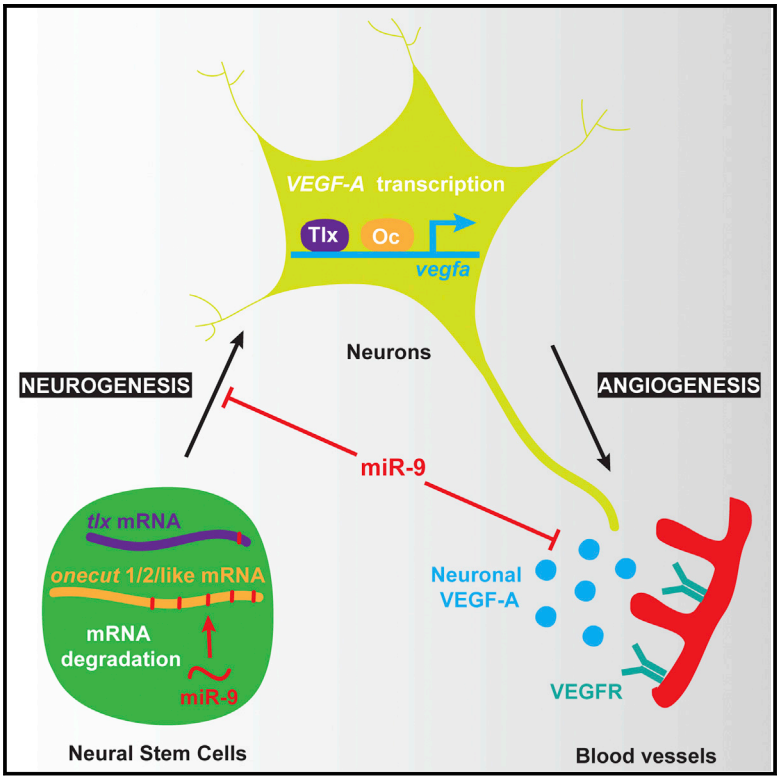

Authors

Romain Madelaine, Steven A. Sloan, Nina Huber, ..., Mark A. Krasnow, Ben A. Barres, Philippe Mourrain

Correspondence

mourrain@stanford.edu

In Brief

The coordination of neuronal and vascular cell development is critical to ensure the proper formation of the vertebrate brain. Madelaine et al. show that the microRNA-9 couples neurogenesis and brain angiogenesis through the inhibition of Tlx and Onecut transcription factors regulating neuronal VEGF-A expression.

Highlights

- VEGF-A is expressed in human differentiated neurons prior to astrogenesis
- miR-9 is expressed in neural stem cells and negatively regulates neuronal VEGF-A
- miR-9-direct targets *TLX* and *ONECUTs* are transcriptional activators of *VEGF-A*
- miR-9 modulation of neuronal VEGF-A controls brain angiogenesis in vivo

Madelaine et al., 2017, Cell Reports *20*, 1533–1542
August 15, 2017 © 2017 The Authors.
http://dx.doi.org/10.1016/j.celrep.2017.07.051

Cell Reports
Report

OPEN ACCESS
CellPress

MicroRNA-9 Couples Brain Neurogenesis and Angiogenesis

Romain Madelaine,[1] Steven A. Sloan,[2] Nina Huber,[1] James H. Notwell,[3] Louis C. Leung,[1] Gemini Skariah,[1] Caroline Halluin,[1] Sergiu P. Paşca,[1] Gill Bejerano,[3,4] Mark A. Krasnow,[5] Ben A. Barres,[2] and Philippe Mourrain[1,6,7,*]
[1]Stanford Center for Sleep Sciences and Medicine, Department of Psychiatry and Behavioral Sciences, Stanford University, Stanford, CA 94305, USA
[2]Department of Neurobiology, Stanford University, Stanford, CA 94305, USA
[3]Department of Computer Science, Stanford University, Stanford, CA 94305, USA
[4]Department of Developmental Biology, Stanford University, Stanford, CA 94305, USA
[5]HHMI and Department of Biochemistry, Stanford University, Stanford, CA 94305, USA
[6]INSERM 1024, École Normale Supérieure, Paris 75005, France
[7]Lead Contact
*Correspondence: mourrain@stanford.edu
http://dx.doi.org/10.1016/j.celrep.2017.07.051

SUMMARY

In the developing brain, neurons expressing VEGF-A and blood vessels grow in close apposition, but many of the molecular pathways regulating neuronal VEGF-A and neurovascular system development remain to be deciphered. Here, we show that miR-9 links neurogenesis and angiogenesis through the formation of neurons expressing VEGF-A. We found that miR-9 directly targets the transcription factors TLX and ONECUTs to regulate *VEGF-A* expression. miR-9 inhibition leads to increased TLX and ONECUT expression, resulting in *VEGF-A* overexpression. This untimely increase of neuronal VEGF-A signal leads to the thickening of blood vessels at the expense of the normal formation of the neurovascular network in the brain and retina. Thus, this conserved transcriptional cascade is critical for proper brain development in vertebrates. Because of this dual role on neural stem cell proliferation and angiogenesis, miR-9 and its downstream targets are promising factors for cellular regenerative therapy following stroke and for brain tumor treatment.

INTRODUCTION

The development of the neurovascular system is essential to ensure proper functioning of the CNS. The vertebrate CNS is predominantly vascularized through the process of angiogenesis, in which proliferating endothelial cells (ECs) form new vessels by sprouting from a pre-existing vascular network (Risau, 1997). Studies across vertebrates have identified many of the conserved cellular and molecular mechanisms underlying CNS vascularization (Gerhardt et al., 2003; Ruhrberg et al., 2002; Stone et al., 1995). To date, the most potent angiogenic intercellular signal identified is the vascular endothelial growth factor (VEGF)-A (Ferrara and Kerbel, 2005; Ruhrberg and Bautch, 2013). VEGF-A gradients guide the ingression and growth of blood vessels within neural tissues (Ruhrberg et al., 2002). During development, VEGF-A is also involved in many aspects of vasculature formation, including sprouting, pruning, connectivity, vessel caliber, and survival (Ruhrberg and Bautch, 2013).

Current models of CNS angiogenesis and neurovascular development are largely glia-centric (Armulik et al., 2010; Bozoyan et al., 2012; Daneman et al., 2010), despite the observation that VEGF-A is expressed in the brain prior to the generation of mature astrocytes during early development (Breier et al., 1992; Wälchli et al., 2015). Importantly, it was also shown that astrocyte-derived VEGF-A is dispensable to retinal vasculature formation (Scott et al., 2010), suggesting a critical role for neuronal VEGF-A in retinal angiogenesis. Consistent with a neuronal function during neurovascular development in the CNS, VEGF-A expression has been observed in multiple types of neurons in different species (D'Amore, 2007; Gerhardinger et al., 1998; Ogunshola et al., 2002; Shima et al., 1996). Further, a functional neuronal contribution has been suggested in the peripheral nervous system, where nerve-derived VEGF can induce arteriogenesis (Mukouyama et al., 2002). However, the exact cell type regulating this process was unclear, as both Schwann cells and sensory neurons forming the peripheral nerve express VEGF. In the spinal cord, one recent report has shown that VEGF-A derived from neurons is required for vascularization (Wild et al., 2017). Despite these observations, how neuronal VEGF-A is regulated and contributes to the formation of the blood vessel network throughout the developing brain remain poorly understood.

In this study, we investigate the coupling role of *microRNA-9* (*miR-9*) activity to neurogenesis and angiogenesis during brain development. *miR-9* expression is detected in neural stem cells (NSCs) (Coolen et al., 2013), and its inhibition transiently increases proliferation, reducing the number of early-born neurons while increasing the number of late-differentiating neurons (Bonev et al., 2011; Coolen et al., 2012; Shibata et al., 2011). Interestingly, miR-9 has also been associated with cancer cell vascularization in vitro (Zhang et al., 2012; Zhuang et al., 2012), suggesting a potential role for this microRNA in physiological angiogenesis in vivo. However, direct evidence has been lacking. Here, we identify a key transcriptional cascade downstream

This is an open access article under the CC BY-NC-ND license (http://creativecommons.org/licenses/by-nc-nd/4.0/).

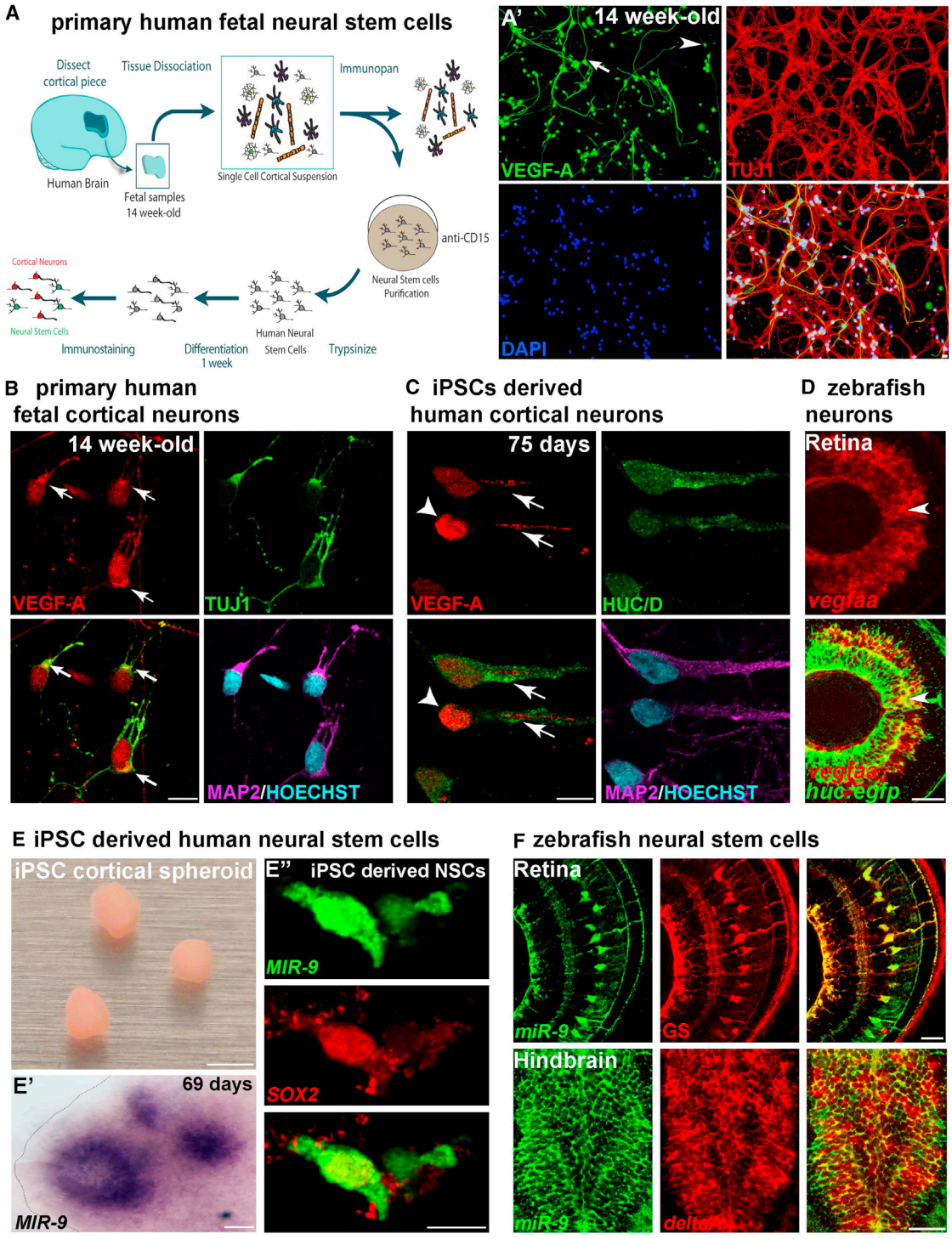

Figure 1. Neuronal VEGF-A and *miR-9* Expression in Neural Stem Cells (NSCs) Are Conserved in the Human Brain

(A) Schematic representation of the method used to obtain primary human NSCs from fetal brain at 14 weeks of development. At 7 days in culture (A'), a majority of the TUJ1-expressing embryonic neurons express detectable levels of VEGF-A (98.5%, n = 201). NSCs (arrow) and neurons (arrowhead) express VEGF-A in primary human cell culture.

(B and C) Confocal sections of primary human cortical neurons (B) and iPSC-derived human cortical neurons (C) immunolabeled with VEGF-A. Young human cortical neurons show heterogeneous localization of VEGF-A (arrows show cytoplasmic and axonal localization; arrowhead indicates strong nuclear expression).

(D) Confocal section of double in situ/immunolabeling showing overlap in the expression of *vegfaa* and *Tg(huc:egfp)* post-mitotic neurons in the retina (arrowheads).

(legend continued on next page)

of miR-9 that regulates neuronally derived VEGF-A. Our results uncover a delicate balance of VEGF-A signaling that controls blood vessel formation, carefully maintained by miR-9 negative regulation of *TLX* and *ONECUT* expression. This study indicates that miR-9-dependent neuronal expression of VEGF-A is a main component of neurovascular system development in the vertebrate brain.

RESULTS

VEGF-A Is Highly Expressed in Neurons before Astrogenesis in the Developing Human Brain

To study early neuronal VEGF-A expression and function, we first investigated the expression pattern of VEGF-A in the developing human brain. We examined cortical neurons purified from 14-gestational-week (14GW) fetal tissue (Figure 1A). At this age of human fetal cortical development, gliogenesis has not yet begun, and the glial fibrillary acidic protein (GFAP)$^+$ cells represent young NSCs (Zhang et al., 2016). We observed robust VEGF-A expression in primary cultures of 14GW human fetal cortical neurons (Figures 1A' and 1B; 98.5%, n = 201) but also in iPSC (induced pluripotent stem cell)-derived neurons (Figure 1C), suggesting that VEGF-A is a hallmark of young neurons and that neuronally derived VEGF-A may have a function during developmental processes. We then extended this mammalian observation to the developing zebrafish. We focused on the hindbrain and retina, two brain structures used as archetype regions for brain vasculature development (Gerhardt et al., 2003; Ruhrberg et al., 2002). We found that, during early (2-day-old) zebrafish development, VEGF-A is expressed in neurons throughout the CNS (retina and hindbrain in Figures 1D and S1A, respectively, and spinal cord in Wild et al., 2017). Consistent with a role for neuronally derived VEGF-A in angiogenesis, we found that the neurovasculature is embedded or in close cellular proximity with axons (Figures S1B–S1H'). Together with the axonal expression of VEGF-A observed in cultured primary and iPSC-derived neurons (Figures 1B and 1C), this observation suggested a possible neuronal influence in vascular morphogenesis. Thus, we hypothesized that neuronally derived VEGF-A is a component of the neurovascular system formation from fish to human.

VEGF-A Expression Is Regulated by miR-9 in the Brain

We reasoned that miR-9 may control vasculature development by modulating the neuronal expression of VEGF-A. Using human iPSC-derived cortical spheroids (Figure 1E), which are 3D cultures resembling the developing human cerebral cortex (Paşca et al., 2015), we identified *MIR-9* expression in NSCs in the *SOX2*$^+$ proliferative zones of the developing human nervous tissue (Figures 1E' and 1E''). Using neural stem cell markers (Chapouton et al., 2010; Coolen et al., 2012; Schmidt et al., 2013), we also confirmed *miR-9* expression in *gfap*$^+$ and *deltaA*$^+$ NSCs in the zebrafish brain (Figures 1F, S2A, and S2B) and uncovered a novel *miR-9* expression in the Müller cells (GS$^+$), the NSCs of the retina (Figure 1F). Because of the conservation of *miR-9* expression in the human and zebrafish developing brains, and its well-known function in neurogenesis, we hypothesized that miR-9 may be an important regulator of neuronal VEGF-A expression.

We next investigated how the expression of VEGF-A might be affected by miR-9, using both miR-9 depletion and miR-9 mimics to decrease and increase miR-9 activity, respectively (Figure 2A). Because of the miR-9 gene duplication (7 genes in teleosts and 3 genes in mammals), genetic manipulation of this microRNA is not simple. Fortunately, all miR-9 genes produce an identical mature 23-bp sequence that can be targeted by a single antisense miR-9 morpholino (MO) (Bonev et al., 2011; Coolen et al., 2012). We found that *vegfa* mRNA accumulation was strongly increased throughout the brain, including retina in the miR-9-depleted larvae, while reduced in miR-9 mimic-injected larvae (Figure 2B). These observations suggest that miR-9 controls directly or indirectly VEGF-A expression during neurovascular development and can potentially regulate blood vessels formation in the brain.

Brain and Retinal Blood Vessel Networks Are Disorganized in Absence of miR-9

The onset of *miR-9* expression in the hindbrain and retina during the second day of zebrafish development is consistent with the formation of the vasculature in these regions (Figures S1B, S1D, and S2C). To investigate the potential coupling of miR-9 activity to neurogenesis and neurovascular development, we inhibited all *miR-9* genes (Figure S3A) in a *kdrl/vegfr2:mCherry* transgenic line that labels the entire vasculature (Chi et al., 2008). While the vascular organization outside of the CNS was normal (Figure S3B), many aspects of the blood vessel network were affected in the brain and retina when miR-9 activity was impeded (Figures 2C, 2D, and S3C). In the brain, the middle mesencephalic central arteries (MMCtAs) were affected in the midbrain, as well as the central arteries (CtAs) in the hindbrain. Similarly, in the retina, the hyaloid vasculature was strongly reduced, but the remaining vessels were thicker. These results suggest a role for miR-9 in brain and retina angiogenesis starting on the second day of development.

As a post-transcriptional regulator, we reasoned that miR-9 may have a dose-dependent effect on brain angiogenesis. In the eye, as the level of miR-9 knockdown decreased, the hyaloid vasculature progressively recovered its mesh-like organization and retinal vessel network cupping the lens (Figures S3D and S3F). In the zebrafish hindbrain, the CtAs sprout from the primordial hindbrain channels (PHBCs) at 32 hours post-fertilization (hpf) (Ulrich et al., 2011), an event concomitant with the onset of miR-9 expression (Coolen et al., 2012). While posterior communicating segments (PCSs) and the basilar artery (BA)

(E) iPSC-derived human cortical spheroid in culture. In situ hybridization showing *MIR-9* expression in the ventricular-like zone of human cortical spheroid (E'). Confocal section of double in situ/immunolabeling showing co-localization of *MIR-9* and *SOX2* in iPSC-derived human NSCs (E'').
(F) Confocal section of double immunolabeling with glutamine synthetase (GS) and EGFP in *Tg(hsa-MIR-9-2:egfp)* retina at 72 hpf, showing *miR-9* expression in retinal NSCs. Confocal section of double in situ/immunolabeling showing overlap in the expression of *deltaA* and EGFP in *Tg(hsa-MIR-9-2:egfp)* hindbrain at 72 hpf. Dorsal view of the brain with anterior up. Lateral view of the retina.
Scale bars: 25 μm in (B) and (C); 100 μm in (D), (E'), and (F); 4 mm in (E); and 10 μm in (A') and (E'').

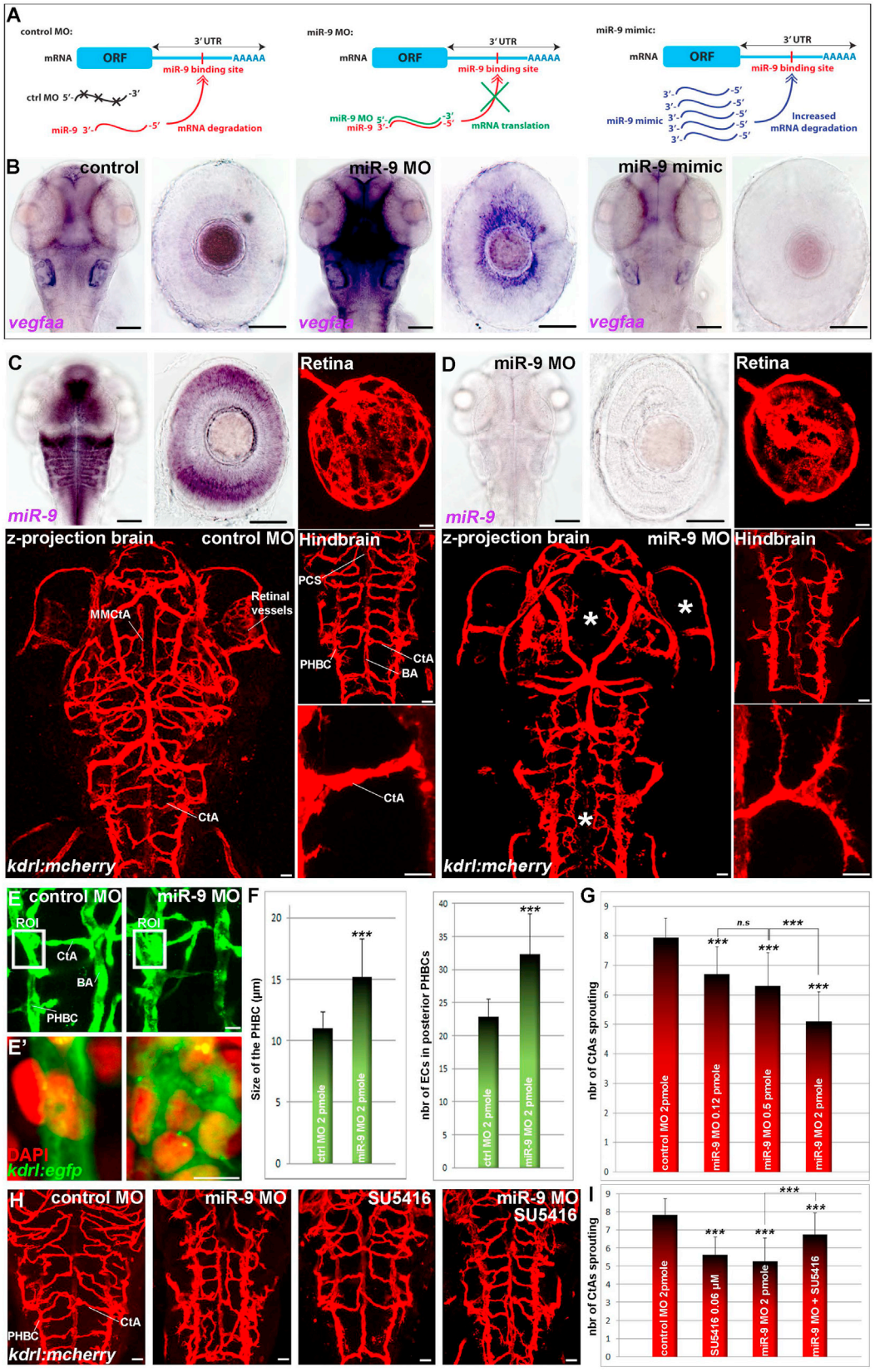

(legend on next page)

were unaffected in miR-9 morphants, CtAs failed to develop normally (Figures 2C and 2D). When they did sprout, CtAs were shorter and/or thinner, displayed multidirectional filopodial extensions, and failed to reach the midline. In contrast to CtAs, PHBCs appeared to be thicker (Figures 2C–2F) and showed an increased diameter when miR-9 was depleted (Figure 2F; 11.1 μm ± 1.3 μm versus 15.2 μm ± 3.2 μm in control and miR-9 morphant, respectively). Furthermore, when miR-9 expression was abolished, we observed an increased number of ECs in PHBCs (22.8 ± 2.7 versus 32.3 ± 6.2 in control and miR-9 morphant, respectively), correlated to a 34% decrease in CtAs sprouting (Figures 2E–2G), suggesting that ECs prematurely differentiated in the PHBCs and/or that their capacity to be recruited to form CtAs was affected. As miR-9 expression was restored, the sprouting of CtAs was progressively recovered (Figures 2G and S3E). These observations are consistent with the previous demonstration that EC migration from PHBCs is the primary mechanism of CtA formation (Ulrich et al., 2011). Altogether, these results indicate that the level of miR-9 activity regulates the formation of the neurovascular system in the brain.

miR-9 Limits VEGF-A Signaling to Regulate Blood Vessel Development

We next hypothesized that VEGF abnormal expression induces the thickening of already formed PHBCs at the expense of the normal formation of CtAs. To test this hypothesis, we used a conditional approach to counteract the excess of VEGF-A signal with SU5416, a specific inhibitor of the VEGF receptor (VEGFR). SU5416 was added in the fish water at 30 hpf, at a very low dose compared to what is used normally to study VEGFR function (Ulrich et al., 2011) (1 μM versus 0.06 μM in our experiment). We chose the lowest dose leading to a vasculature defect to validate that the VEGF signal was at least partially impaired (Figures 2H and 2I). We observed that a moderate inhibition of the VEGF signal in the miR-9-depleted larvae at the onset of CtA angiogenesis (SU5416; 0.06 μM, from 30 hpf to 72 hpf) efficiently rescued the large majority of the blood vessel network (Figures 2H and 2I; 86% versus 67% with the miR-9 MO only, compared to 100% in control morphant). This result shows that miR-9 directly or indirectly limits VEGF-A/VEGFR signal which, in turn, controls normal sprouting of new blood vessels from the preexisting vascular network.

TLX and ONECUTs Are Conserved Direct Targets of miR-9 In Vivo

Because we found that no VEGF ligand genes harbor miR-9 target sites in their 3′ UTR, we utilized a computational approach (Bartel, 2009) to identify targets of miR-9 acting upstream of *VEGF-A*. We identified a number of gene expression regulators that contain miR-9 target sites and that were conserved from human to zebrafish: *ONECUT1*, *ONECUT2*, *LIN28*, *FOXP1*, *FOXP2*, *FOXP4*, and *TLX/NR2E1*. Among these candidates, only *tlx/nr2e1*, *onecut1*, *onecut2*, and *onecut-like* (human *OC2* ortholog in zebrafish) mRNA expression levels demonstrated miR-9 dependence in vivo (Figures S4A–S4D). *tlx* and *onecut1* 3′ UTRs each bear a single miR-9 target site that we validated in vivo by using target protection (TP) experiments and fluorescent sensor assays (Figures 3A–3C and S4E; Zhao et al., 2009). In the case of *onecut2* and *onecut-like*, we identified 12 and 5 potential miR-9 binding sites in their respective 3′ UTRs (Figures 3D and S4D). In the presence of miR-9 mimics, we observed a 56% decrease in EGFP expression fused to the 3′ UTR of *onecut-like* (Figure S4F). Finally, using TP, we validated the direct interaction with one miR-9 site particularly conserved between *ONECUT2* orthologs across vertebrates and between *onecut2* and *onecut-like* paralogs in zebrafish (Figures 3A and 3D). Our results demonstrate in vivo that *tlx* and *onecut* transcription factor mRNAs are direct conserved targets of miR-9 in the vertebrate brain.

TLX and ONECUT Regulate *VEGF-A* Transcriptional Expression In Vivo

Because human and zebrafish *VEGF-A* promoters carry putative TLX and ONECUT binding sites, we next investigated the capacity of these transcription factors to mediate the miR-9-dependent effect on *vegfa* expression. In zebrafish gastrulae, we expressed *tlx* and *onecut* open reading frames (ORFs) under

Figure 2. miR-9 Controls Brain Vasculature Development by Limiting VEGF-A Expression

(A) Schematic representation of the miR-9 MO and miR-9 RNA mimic effects. In the presence of the miR-9 MO, miR-9 is paired with the MO, inhibiting the mRNA degradation. The miR-9 RNA mimic is ubiquitously expressed to allow the degradation of the miR-9 targets.

(B) Whole-mount in situ hybridization against *vegfaa* in embryos at 48 hpf. *vegfaa* mRNA behaves like a miR-9 target, showing an increase in the miR-9 knockdown and a decrease in the miR-9 gain of function.

(C and D) Whole-mount in situ hybridization against *miR-9* in control (C) and miR-9 morphant (D) shows that miR-9 knockdown does not affect brain and eye morphogenesis at 72 hpf. In miR-9 morphant *Tg(kdrl:mCherry)* brain at 72 hpf, the mesencephalic central artery (MMCtA), hindbrain and retinal blood vessels are affected (asterisks in D). In the hindbrain, primordial hindbrain channels (PHBCs) are thicker, and central arteries (CtAs) are disorganized and thinner and show aberrant multidirectional sprouting.

(E) Confocal projections of EGFP labeling in *Tg(kdrl:egfp)* at 72 hpf showing ECs (E'; EGFP+/DAPI+) in posterior PHBCs in control or miR-9 morphant larvae.

(F) Quantification of the size, in microns, of PHBCs (the region of interest [ROI] indicated in E) (control, n = 33; or miR-9 MO, n = 28) and the total number of ECs recruited to form the posterior PHBCs (control, n = 12; or miR-9 MO, n = 10) at 72 hpf.

(G) Quantification of the number of CtAs found on each hemi-hindbrain in the control (n = 20) or the miR-9 MO dilution series (ns = 34, 28, and 56 for croissant dilutions) at 72 hpf.

(H and I) *Tg(kdrl:mCherry)* brain at 72 hpf showing blood vessel formation in the hindbrain (H), and quantification of the number of CtAs found on each hemi-hindbrain (I), of control larvae (n = 40), SU5416-treated larvae (0.06 μM; n = 48), miR-9-morphant larvae (n = 48), and miR-9-MO larvae treated with 0.06 μM SU5416 (n = 30). Dorsal view of the brain with anterior up. Lateral view of the retina.

Scale bars: 100 μm for in situ hybridization (ISH) in (B)–(D) and 10 μm for immunolabeling in (C)–(E') and (H). Error bars represent SD. ***$p < 0.0005$, determined by t test, two-tailed; n.s, not significant.

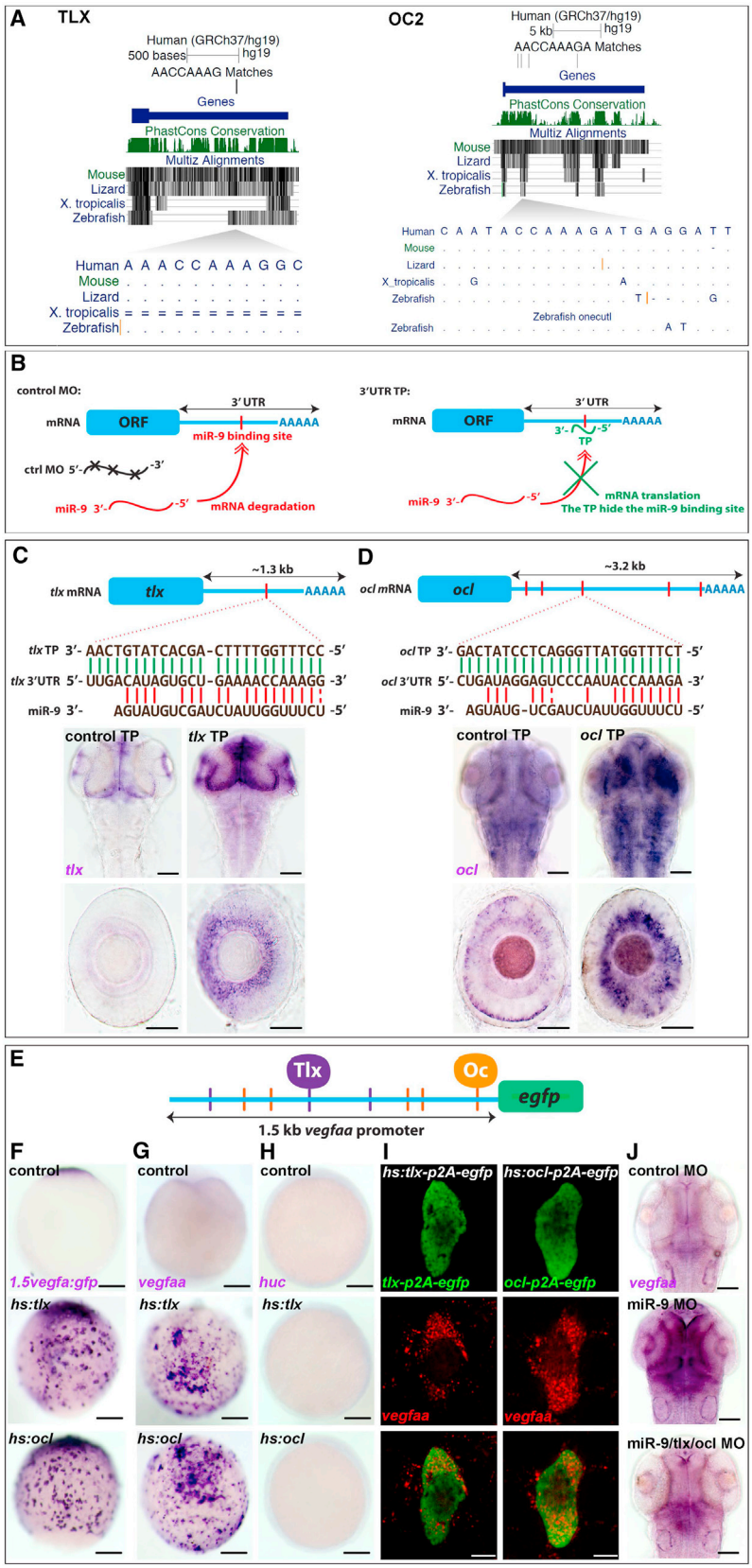

Figure 3. *tlx* and *onecut* Are Direct miR-9 Targets Regulating *VEGF-A* Transcriptional Expression In Vivo

(A) Alignments of vertebrate TLX and ONECUT2 orthologs show strong conservation in the 3′ UTR containing a putative miR-9 binding site.

(B) Schematic representation of the TP assay. In the presence of the TP, the miR-9 binding site is not accessible and the mRNA degradation is inhibited.

(C and D) Schematic representation of the zebrafish *tlx* (C) and *ocl* (D) mRNA indicating the sequence of the putative miR-9 binding site in the 3′ UTR (red) and the alignment with miR-9 or TP. *tlx* and *ocl* mRNA behave like direct miR-9 targets, showing an increase in the TP context.

(E) Schematic representation highlighting putative Tlx (NAGTCA/purple) (Qu et al., 2010; Yu et al., 2000) and Onecut (NN(A/G)TC(A/C)A(T/G)NN/orange) (Lannoy et al., 1998; Plaisance et al., 2006) binding sites in 1.5 kb of the *vegfaa* promoter.

(F) Whole-mount in situ hybridization against *egfp* driven by 1.5 kb of the *vegfaa* promoter. Embryos were injected with *vegfaa:egfp* only, *hs:tlx*, or *hs:ocl* and were heat-shocked at 7 hpf. Embryos display ectopic expression of the *egfp* mRNA 2 hr after treatment, showing that Tlx and Onecut have the ability to induce the transcription via 1.5 kb of the *vegfaa* promoter.

(G and H) Whole-mount in situ hybridization against *vegfaa* (G) and *huc* (H) in embryos at 9 hpf. Embryos were injected with *hs:tlx* or *hs:ocl* and heat-shocked at 7 hpf. Embryos display ectopic expression of *vegfaa*, but not *huc*, 2 hr after treatment, showing that Tlx and Onecut transcription factors have the ability to induce the transcription of the endogenous *vegfaa* gene independently of the neuronal fate.

(I) Mosaic expression of Tlx-p2A-EGFP or Ocl-p2A-EGFP by heat shock at 8.5 hpf induces endogenous *vegfaa* expression in as little as 30 min in a cell-autonomous manner, suggesting a direct regulation.

(J) Whole-mount in situ hybridization against *vegfaa* in embryos at 48 hpf injected with the control MO, miR-9 MO, or miR-9 MO with *tlx* and *ocl* MOs. Dorsal view with anterior up. Lateral view of the retina.

Scale bars: 100 μm in (C), (D), (F)–(H), and (J) or 10 μm in (I).

the control of a heat-shock promoter. We assessed their impact on the expression of endogenous *vegfa* or an *egfp* reporter driven by a compact *vegfa* promoter (Figure 3E). After heat shock, we observed widespread expression of *vegfa* and *egfp* transcripts. These results indicated that both Tlx and Onecut are sufficient to induce endogenous *vegfa* and exogenous *egfp* transcription in vivo (Figures 3F and 3G). We next verified, using a *huc* staining, that no neurons were formed following Tlx or Onecut expression (Figure 3H), demonstrating that *vegfa* transcription is induced independently of the acquisition of a neuronal fate. We then performed a similar set of experiments where a p2A-EGFP cleavable reporter was fused to Tlx and Oc proteins to determine the cell-autonomous transcriptional activation of the *vefga* gene. We observed co-localization of *vegfa* mRNA with EGFP in as little as 15 min after a 15-min heat shock, demonstrating fast cell-autonomous transcriptional activation of *vegfa* by Tlx and Oc (Figure 3I). We then inhibited Tlx and Oc expression in miR-9-depleted embryos and observed a reduced induction of *vegfa* expression (Figure 3J), further supporting Tlx and Oc endogenous roles downstream of miR-9 and upstream of *vegfa* expression.

TLX and ONECUT Promote the Differentiation of Neurons Expressing VEGF-A

TLX and OC expression can be detected in NSCs and neurons (Sapkota et al., 2014; Shi et al., 2004; Yuan et al., 2015; Zhang et al., 2016) (http://www.brainrnaseq.org), and we showed in zebrafish that their expression in NSCs is strongly reduced when miR-9 is robustly expressed in these cells (Figure S5). These observations suggested a role for these transcription factors in NSC differentiation into neurons across vertebrates. First, we studied the role of these transcription factors using primary human fetal NSCs at 14GW, a stage where no differentiated astrocytes are present in the human brain. We transfected purified human embryonic NSCs (hENSCs) with plasmids for EGFP, TLX-p2A-EGFP, or OC2-p2A-EGFP and allowed them to differentiate in culture for 1 week. For TLX-p2A-EGFP- and OC2-p2A-EGFP-transfected cells, we observed that the NSC pool was substantially depleted (Figure S6A; 0.8% and 2.4%, respectively, versus 15.2% in the control). Interestingly, this reduction of ~90% in the number of NSCs is not correlated to a reduction in the number of TUJ1$^+$ cells, but to a 9% increase of neurons expressing VEGF-A (Figures S6A and S6B). Because of the limited access to human fetal tissue, we next investigated the capacity of the miR-9/Tlx/Oc cascade to control neurogenesis in zebrafish. Similarly to human cell culture observation, miR-9 depletion in zebrafish dramatically decreases the pool of NSCs in both brain and retina while increasing *deltaA*$^+$ and *ascl1a*$^+$ neural progenitors and *huc*$^+$ neurons (Figures S6C and S6D), as previously described (Coolen et al., 2012). We also observed that Tlx or Ocl expression in zebrafish NSCs reduces GS expression and that when *tlx* and *ocl* mRNAs are preserved from miR-9-induced decay, *deltaA*$^+$ neural progenitors are increased in the developing brain (Figures S6C and S6D). Together, these results validate the neurogenic function of TLX and OC downstream of miR-9 and suggest that embryonic NSC depletion results from a transition into neuronal fates, promoting the differentiation of neurons expressing VEGF-A.

Neuronal Expression of VEGF-A Induced by TLX and ONECUT Controls Brain Vascular Development

To test whether TLX/OC-dependent VEGF-A expression controls vascular formation in the developing CNS, we expressed these transcription factors under the control of a neuronal promoter (using the *Tg(alpha-tubulin:gal4)* line and the GAL4/UAS system) and also used TP to stabilize endogenous *tlx* and *onecut* mRNAs. In both experiments, Tlx or Oc exogenous and endogenous expression induced *vegfa* upregulation, associated with a reduction of CtAs sprouting (Figures 4A–4D and S7). We also observed an additive impact of Tlx and Oc on *vegfa* expression and angiogenesis defects. These results provide in vivo evidence that miR-9 can control neurovascular development by directly inhibiting *tlx* and *onecut* expression and repressing the VEGF-A pathway.

Finally, to further validate that TLX and OC effects on neurovascular development are mediated through neuronal VEGF-A expression, we expressed VEGF-A in neurons using the *alpha-tubulin:gal4* transgenic line. Consistent with the pro-angiogenic role of VEGF-A, we showed that overexpression of *vegfa* in neurons led to a global hyperplasia of blood vessels in the brain (Figure 4E), but some vessels like MMCtAs in the midbrain are missing (Figure 4E'). In the hindbrain, we observed a 54% decrease in CtAs sprouting, while PHBCs appear thicker (Figures 4E'' and 4F). Similarly, in the retina, the development of the hyaloid vasculature is affected, and retinal vessels are largely missing (Figures 4E and 4E'). Thus, the effect of *vegfa* neuronal expression on blood vessel development was reminiscent of the miR-9-depletion phenotype. This observation suggests that the increase in angiogenesis from the preexisting vascular network affects the availability/capability of ECs to form subsequent new blood vessels during development. Overall, these results uncover a conserved miR-9-dependent cascade regulating VEGF-A expression (Figure 4G) and indicate that neuronally derived VEGF-A is a critical angiogenic factor in the developing vertebrate brain.

DISCUSSION

Neuronal VEGF-A Is an Angiogenic Factor during Early Brain Development in Human

Consistent with a neuronal role in angiogenesis in the developing human brain, our data show that VEGF-A is highly expressed by human fetal primary neurons at a time when no differentiated astrocytes are detected (14 gestational weeks in human fetal cortices). This may represent the major source of VEGF-A necessary for neurovasculature formation during early development. In comparison to radial glia, cortical neurons display a much weaker immunostaining for VEGF-A proteins, but because neurons are much more abundant during early CNS development, the gross VEGF signal produced by these cells may be entirely sufficient for normal vascularization. Our data showing that iPSC-derived neurons within human cortical spheroids (which are not vascularized) express VEGF-A indicate that neuronal VEGF-A expression is a part of the genetic program controlling neuronal identity and is not solely a response to angiogenic processes. Interestingly, in both primary neurons and iPSC-derived neurons, we detected a dual

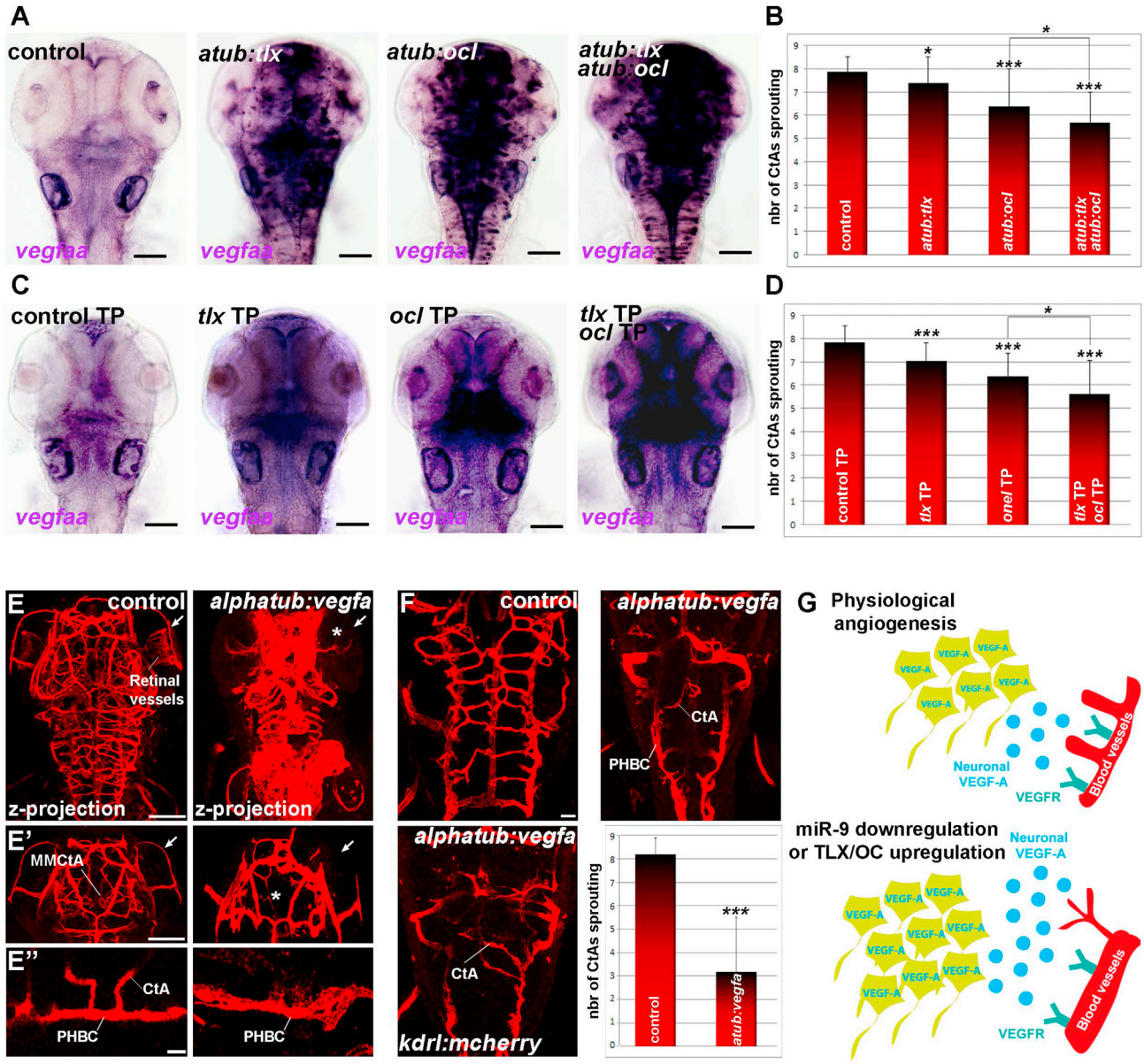

Figure 4. Tlx- and Oc-Dependent Neuronal Expression of VEGF-A Affect Brain Vasculature Development

(A) Whole-mount in situ hybridization against *vegfaa* at 48 hpf in controls or embryos expressing *uas:tlx*, *uas:ocl*, or *uas:tlx* and *uas:ocl* in a pan-neuronal manner in *Tg(alpha-tubulin:gal4)*.

(B) Quantification of the number of CtAs found on each hemi-hindbrain in controls (n = 34) or larvae expressing *uas:tlx* (n = 46), *uas:ocl* (n = 46) or *uas:tlx* and *uas:ocl* (n = 46) in a pan-neuronal manner in *Tg(alpha-tubulin:gal4)* at 72 hpf.

(C) Whole-mount in situ hybridization against *vegfaa* in embryos at 48 hpf injected with the control MO, *tlx* TP, *ocl* TP, or *tlx* and *ocl* TP.

(D) Quantification of the number of CtAs found on each hemi-hindbrain in the control MO (n = 32), *tlx* TP (n = 34), *ocl* TP (n = 34), or *tlx* and *ocl* TP (n = 34) larvae at 72 hpf.

(E) Neuronal expression of VEGF-A in the *Tg(alpha-tubulin:gal4)* line leads to a global increase in ECs and/or blood vessel formation in the brain at 72 hpf. While most of the vessels appear to be thicker, the mesencephalic central artery (MMCtA) and retinal blood vessels are reduced or missing (arrow and asterisk in E and E'). In the hindbrain, PHBCs are thicker, while CtA sprouting is reduced, suggesting that their development is affected following neuronal VEGF-A expression (E'').

(F) Quantification of the number of CtAs found on each hemi-hindbrain in controls (n = 30) and larvae expressing *vegfaa* (n = 20) in neurons at 72 hpf.

(G) During the normal development of the neurovascular system, miR-9 represses the expression of Tlx and Oc to limit the level of neuronally derived VEGF-A. A reduction of miR-9 expression and/or an overexpression of Tlx/Oc increases the level of neuronal VEGF-A and affects the development of the brain vasculature. Dorsal view of the brain with anterior up.

Scale bars: 100 μm in (A), (C), (E), and (E') or 10 μm in (F) and (E''). Error bars represent SD. *$p < 0.05$; ***$p < 0.0005$, determined by t test, two-tailed.

localization of VEGF-A in the nucleus and in vesicular structures of the cytoplasm, suggesting that, in addition to its *trans* activity through VEGF Receptor-2 activation, VEGF-A may also have unappreciated biological functions, such as transcriptional control of gene expression via a cell-autonomous mechanism, as demonstrated for VEGF-D in human lung fibroblasts (El-Chemaly et al., 2014).

miR-9 Is a Critical Factor Coupling Neurogenesis and Angiogenesis

The coordination of neurogenesis and angiogenesis is critical to the proper formation of the vertebrate brain, and the control of VEGF-A expression by the neurogenesis modulator miR-9 reveals a conserved transcriptional cascade linking neuronal and vascular development. Two previous studies have reported a link between miR-9 and tumor angiogenesis in vitro, but the physiological significance of the reported mechanisms was unclear, because these reports produced paradoxical results: showing a pro-angiogenic activity of miR-9 via the JAK-STAT pathway in one case (Zhuang et al., 2012) and an anti-angiogenic activity via matrix metalloproteinase 14 in the other (Zhang et al., 2012). Here, we demonstrated that miR-9 is regulating angiogenesis in vivo by decreasing the stability of *tlx* and *onecut* mRNAs to limit neuronal VEGF-A signaling. The constitutive neuronal expression of both Tlx and Oc using a neuronal driver led to vasculature defects similarly to neuronal *VEGF-A* expression, demonstrating their capacities to control *VEGF-A* transcription in neurons downstream of miR-9 to regulate brain and retina angiogenesis. These findings are significant for our understanding of the early vascularization in the CNS but also to identify molecular targets for anti-VEFG therapies in retinal diseases and brain tumors.

EXPERIMENTAL PROCEDURES

Fish Developmental Conditions and Immunostaining

Embryos were raised and staged according to standard protocols (Kimmel et al., 1995). Our animal protocol (#9935) is approved by the American Association for the Accreditation of Laboratory Animal Care (AAALAC) in accordance with Stanford University animal care guidelines. Embryos were fixed overnight at 4°C in 4% paraformaldehyde (PFA), after which they were dehydrated in ethanol. Immunostainings were performed using anti-GFP (1/1,000, Torrey Pines Biolabs), anti-HuC/D (1/500, Molecular Probes), anti-DsRed (1/500, Clontech Laboratories), anti-GS (1/500, Fisher Scientific), and anti-Acetylated Tubulin (1/500, Sigma) as primary antibodies and Alexa 488- or Alexa 555-conjugated goat anti-rabbit immunoglobulin G (IgG) or goat anti-mouse IgG (1/1,000) as secondary antibody (Molecular Probes).

Primary Human Embryonic NSC Immunostaining

Purified NSCs were obtained from 14-week-old human fetal brains (institutional review board [IRB] approval under Protocol #20083). For immunostaining, coverslips were fixed in 4% PFA for 10 min before blocking with 10% goat serum and 0.1% Triton X-100 for 30 min. The primary antibodies include GFAP (1/1,500, Dako), Tuj1 (1/1,500, Covance), VEGF-A (1/50, Santa Cruz Biotechnology), and GFP (1/1,000, Abcam). Coverslips were incubated with primary antibody overnight in blocking solution, washed in PBS, and then incubated with secondary antibodies (Alexa) in blocking solution for 90 min prior to mounting.

Human iPSC-Derived Cortical Neuron Immunostaining

Human cortical spheroids (hCSs) were generated from human iPSCs as previously described (Paşca et al., 2015). The generation of iPSCs was approved by the Stanford IRB. Fibroblasts for reprogramming were collected and deidentified following informed consent. For immunostaining, the samples were fixed in 4% PFA for 10 min before blocking with 10% goat serum and 0.3% Triton X-100 for 1 hr. Samples were incubated with primary antibodies anti-VEGF-A (1/100, Santa Cruz), anti-HuC/D (1/400, Life Technologies), and anti-MAP2 (1/1500, Synaptic Systems) in 10% goat serum for 2 hr, washed with PBS, and incubated with secondary antibodies (Alexa-conjugated; Life Technologies) in 10% goat serum for 45 min prior to mounting.

Image Acquisition Cell Counting and Blood Vessel Quantification

Confocal images were acquired using a Leica SP5 confocal microscope or a Leica TCS SP8 confocal microscope (Stanford Cell Sciences Imaging Facility). Images were prepared using Photoshop (Adobe). For cell counting and blood vessel quantification, images were analyzed using ImageJ software. Statistical analyses associated with each figure are reported in the figure legends.

SUPPLEMENTAL INFORMATION

Supplemental Information includes Supplemental Experimental Procedures and seven figures and can be found with this article online at http://dx.doi.org/10.1016/j.celrep.2017.07.051.

AUTHOR CONTRIBUTIONS

R.M. and P.M. designed and analyzed in vivo experiments. R.M. performed in vivo experiments with the assistance of G.S. and C.H. L.C.L. established the *Tg(gfap:gal4)* line. S.A.S., N.H., R.M., S.P.P., B.A.B., and P.M. designed and analyzed in vitro experiments. S.A.S and N.H. performed in vitro experiments. J.H.N. and G.B. performed in silico analysis. M.A.K. advised on the blood vessel study. R.M., S.A.S., J.H.N., G.B., B.A.B., and P.M wrote the manuscript. P.M. supervised the entire study.

ACKNOWLEDGMENTS

We thank members of the Mourrain, Barres, and Bejerano laboratories for insightful discussions. We are grateful to Drs. Pamela A. Raymond, Neil C. Chi, David Traver, Holger Knaut, Maximiliano L. Suster, William S. Talbot, Thomas S. Becker, Shawn M. Burgess, Jeffrey L. Goldberg, and Nathan Lawson for the gift of reagents or helpful discussions. We would also like to thank the Stanford CSIF Imaging platform.

This work was supported by grants from the NIH to P.M. (NS062798, DK090065, and MH099647), G.B. (HG005058), S.A.S. (F30MH106261 and T32GM007365), and B.A.B. (MH099555-03). P.M. was also supported by the BrightFocus Foundation. R.M. was supported by an EMBO Long-Term Fellowship (ALTF 413-2012) and the BrightFocus Foundation. J.H.N. was supported by a National Science Foundation Fellowship (DGE-1147470) and a Bio-X Stanford Interdisciplinary Graduate Fellowship. S.A.S. was supported by a Bio-X-Stanford Predoctoral Fellowship. G.B. was supported by a Packard Fellowship. N.H. was supported by a Stanford Dean's Postdoctoral Fellowship and Child Health Research Institute Postdoctoral Fellowship UL1-TR001085. S.P.P. was supported by the NIMH BRAINS Award (R01MH107800), the MQ Fellow Award, a Donald E. and Delia B. Baxter Foundation Award, and the Kwan Foundation.

Received: March 30, 2017
Revised: June 30, 2017
Accepted: July 19, 2017
Published: August 15, 2017

REFERENCES

Armulik, A., Genové, G., Mäe, M., Nisancioglu, M.H., Wallgard, E., Niaudet, C., He, L., Norlin, J., Lindblom, P., Strittmatter, K., et al. (2010). Pericytes regulate the blood-brain barrier. Nature *468*, 557–561.

Bartel, D.P. (2009). MicroRNAs: target recognition and regulatory functions. Cell *136*, 215–233.

Bonev, B., Pisco, A., and Papalopulu, N. (2011). MicroRNA-9 reveals regional diversity of neural progenitors along the anterior-posterior axis. Dev. Cell *20*, 19–32.

Bozoyan, L., Khlghatyan, J., and Saghatelyan, A. (2012). Astrocytes control the development of the migration-promoting vasculature scaffold in the postnatal brain via VEGF signaling. J. Neurosci. *32*, 1687–1704.

Breier, G., Albrecht, U., Sterrer, S., and Risau, W. (1992). Expression of vascular endothelial growth factor during embryonic angiogenesis and endothelial cell differentiation. Development *114*, 521–532.

Chapouton, P., Skupien, P., Hesl, B., Coolen, M., Moore, J.C., Madelaine, R., Kremmer, E., Faus-Kessler, T., Blader, P., Lawson, N.D., and Bally-Cuif, L. (2010). Notch activity levels control the balance between quiescence and recruitment of adult neural stem cells. J. Neurosci. *30*, 7961–7974.

Chi, N.C., Shaw, R.M., De Val, S., Kang, G., Jan, L.Y., Black, B.L., and Stainier, D.Y. (2008). Foxn4 directly regulates tbx2b expression and atrioventricular canal formation. Genes Dev. *22*, 734–739.

Coolen, M., Thieffry, D., Drivenes, Ø., Becker, T.S., and Bally-Cuif, L. (2012). miR-9 controls the timing of neurogenesis through the direct inhibition of antagonistic factors. Dev. Cell *22*, 1052–1064.

Coolen, M., Katz, S., and Bally-Cuif, L. (2013). miR-9: a versatile regulator of neurogenesis. Front. Cell. Neurosci. *7*, 220.

D'Amore, P.A. (2007). Vascular endothelial cell growth factor-a: not just for endothelial cells anymore. Am. J. Pathol. *171*, 14–18.

Daneman, R., Zhou, L., Kebede, A.A., and Barres, B.A. (2010). Pericytes are required for blood-brain barrier integrity during embryogenesis. Nature *468*, 562–566.

El-Chemaly, S., Pacheco-Rodriguez, G., Malide, D., Meza-Carmen, V., Kato, J., Cui, Y., Padilla, P.I., Samidurai, A., Gochuico, B.R., and Moss, J. (2014). Nuclear localization of vascular endothelial growth factor-D and regulation of c-Myc-dependent transcripts in human lung fibroblasts. Am. J. Respir. Cell Mol. Biol. *51*, 34–42.

Ferrara, N., and Kerbel, R.S. (2005). Angiogenesis as a therapeutic target. Nature *438*, 967–974.

Gerhardinger, C., Brown, L.F., Roy, S., Mizutani, M., Zucker, C.L., and Lorenzi, M. (1998). Expression of vascular endothelial growth factor in the human retina and in nonproliferative diabetic retinopathy. Am. J. Pathol. *152*, 1453–1462.

Gerhardt, H., Golding, M., Fruttiger, M., Ruhrberg, C., Lundkvist, A., Abramsson, A., Jeltsch, M., Mitchell, C., Alitalo, K., Shima, D., and Betsholtz, C. (2003). VEGF guides angiogenic sprouting utilizing endothelial tip cell filopodia. J. Cell Biol. *161*, 1163–1177.

Kimmel, C.B., Ballard, W.W., Kimmel, S.R., Ullmann, B., and Schilling, T.F. (1995). Stages of embryonic development of the zebrafish. Dev. Dyn. *203*, 253–310.

Lannoy, V.J., Bürglin, T.R., Rousseau, G.G., and Lemaigre, F.P. (1998). Isoforms of hepatocyte nuclear factor-6 differ in DNA-binding properties, contain a bifunctional homeodomain, and define the new ONECUT class of homeodomain proteins. J. Biol. Chem. *273*, 13552–13562.

Mukouyama, Y.S., Shin, D., Britsch, S., Taniguchi, M., and Anderson, D.J. (2002). Sensory nerves determine the pattern of arterial differentiation and blood vessel branching in the skin. Cell *109*, 693–705.

Ogunshola, O.O., Antic, A., Donoghue, M.J., Fan, S.Y., Kim, H., Stewart, W.B., Madri, J.A., and Ment, L.R. (2002). Paracrine and autocrine functions of neuronal vascular endothelial growth factor (VEGF) in the central nervous system. J. Biol. Chem. *277*, 11410–11415.

Paşca, A.M., Sloan, S.A., Clarke, L.E., Tian, Y., Makinson, C.D., Huber, N., Kim, C.H., Park, J.Y., O'Rourke, N.A., Nguyen, K.D., et al. (2015). Functional cortical neurons and astrocytes from human pluripotent stem cells in 3D culture. Nat. Methods *12*, 671–678.

Plaisance, V., Abderrahmani, A., Perret-Menoud, V., Jacquemin, P., Lemaigre, F., and Regazzi, R. (2006). MicroRNA-9 controls the expression of Granuphilin/Slp4 and the secretory response of insulin-producing cells. J. Biol. Chem. *281*, 26932–26942.

Qu, Q., Sun, G., Li, W., Yang, S., Ye, P., Zhao, C., Yu, R.T., Gage, F.H., Evans, R.M., and Shi, Y. (2010). Orphan nuclear receptor TLX activates Wnt/beta-catenin signalling to stimulate neural stem cell proliferation and self-renewal. Nat. Cell Biol. *12*, 31–40.

Risau, W. (1997). Mechanisms of angiogenesis. Nature *386*, 671–674.

Ruhrberg, C., and Bautch, V.L. (2013). Neurovascular development and links to disease. Cell. Mol. Life Sci. *70*, 1675–1684.

Ruhrberg, C., Gerhardt, H., Golding, M., Watson, R., Ioannidou, S., Fujisawa, H., Betsholtz, C., and Shima, D.T. (2002). Spatially restricted patterning cues provided by heparin-binding VEGF-A control blood vessel branching morphogenesis. Genes Dev. *16*, 2684–2698.

Sapkota, D., Chintala, H., Wu, F., Fliesler, S.J., Hu, Z., and Mu, X. (2014). Onecut1 and Onecut2 redundantly regulate early retinal cell fates during development. Proc. Natl. Acad. Sci. USA *111*, E4086–E4095.

Schmidt, R., Strähle, U., and Scholpp, S. (2013). Neurogenesis in zebrafish – from embryo to adult. Neural Dev. *8*, 3.

Scott, A., Powner, M.B., Gandhi, P., Clarkin, C., Gutmann, D.H., Johnson, R.S., Ferrara, N., and Fruttiger, M. (2010). Astrocyte-derived vascular endothelial growth factor stabilizes vessels in the developing retinal vasculature. PLoS ONE *5*, e11863.

Shi, Y., Chichung Lie, D., Taupin, P., Nakashima, K., Ray, J., Yu, R.T., Gage, F.H., and Evans, R.M. (2004). Expression and function of orphan nuclear receptor TLX in adult neural stem cells. Nature *427*, 78–83.

Shibata, M., Nakao, H., Kiyonari, H., Abe, T., and Aizawa, S. (2011). MicroRNA-9 regulates neurogenesis in mouse telencephalon by targeting multiple transcription factors. J. Neurosci. *31*, 3407–3422.

Shima, D.T., Gougos, A., Miller, J.W., Tolentino, M., Robinson, G., Adamis, A.P., and D'Amore, P.A. (1996). Cloning and mRNA expression of vascular endothelial growth factor in ischemic retinas of Macaca fascicularis. Invest. Ophthalmol. Vis. Sci. *37*, 1334–1340.

Stone, J., Itin, A., Alon, T., Pe'er, J., Gnessin, H., Chan-Ling, T., and Keshet, E. (1995). Development of retinal vasculature is mediated by hypoxia-induced vascular endothelial growth factor (VEGF) expression by neuroglia. J. Neurosci. *15*, 4738–4747.

Ulrich, F., Ma, L.H., Baker, R.G., and Torres-Vázquez, J. (2011). Neurovascular development in the embryonic zebrafish hindbrain. Dev. Biol. *357*, 134–151.

Wälchli, T., Wacker, A., Frei, K., Regli, L., Schwab, M.E., Hoerstrup, S.P., Gerhardt, H., and Engelhardt, B. (2015). Wiring the vascular network with neural cues: A CNS perspective. Neuron *87*, 271–296.

Wild, R., Klems, A., Takamiya, M., Hayashi, Y., Strähle, U., Ando, K., Mochizuki, N., van Impel, A., Schulte-Merker, S., Krueger, J., et al. (2017). Neuronal sFlt1 and Vegfaa determine venous sprouting and spinal cord vascularization. Nat. Commun. *8*, 13991.

Yu, R.T., Chiang, M.Y., Tanabe, T., Kobayashi, M., Yasuda, K., Evans, R.M., and Umesono, K. (2000). The orphan nuclear receptor Tlx regulates Pax2 and is essential for vision. Proc. Natl. Acad. Sci. USA *97*, 2621–2625.

Yuan, J., Lei, Z.N., Wang, X., Deng, Y.J., and Chen, D.B. (2015). Interaction between Oc-1 and Lmx1a promotes ventral midbrain dopamine neural stem cells differentiation into dopamine neurons. Brain Res. *1608*, 40–50.

Zhang, H., Qi, M., Li, S., Qi, T., Mei, H., Huang, K., Zheng, L., and Tong, Q. (2012). microRNA-9 targets matrix metalloproteinase 14 to inhibit invasion, metastasis, and angiogenesis of neuroblastoma cells. Mol. Cancer Ther. *11*, 1454–1466.

Zhang, Y., Sloan, S.A., Clarke, L.E., Caneda, C., Plaza, C.A., Blumenthal, P.D., Vogel, H., Steinberg, G.K., Edwards, M.S., Li, G., et al. (2016). Purification and characterization of progenitor and mature human astrocytes reveals transcriptional and functional differences with mouse. Neuron *89*, 37–53.

Zhao, C., Sun, G., Li, S., and Shi, Y. (2009). A feedback regulatory loop involving microRNA-9 and nuclear receptor TLX in neural stem cell fate determination. Nat. Struct. Mol. Biol. *16*, 365–371.

Zhuang, G., Wu, X., Jiang, Z., Kasman, I., Yao, J., Guan, Y., Oeh, J., Modrusan, Z., Bais, C., Sampath, D., and Ferrara, N. (2012). Tumour-secreted miR-9 promotes endothelial cell migration and angiogenesis by activating the JAK-STAT pathway. EMBO J. *31*, 3513–3523.

Cell Reports, Volume *20*

Supplemental Information

MicroRNA-9 Couples Brain

Neurogenesis and Angiogenesis

Romain Madelaine, Steven A. Sloan, Nina Huber, James H. Notwell, Louis C. Leung, Gemini Skariah, Caroline Halluin, Sergiu P. Paşca, Gill Bejerano, Mark A. Krasnow, Ben A. Barres, and Philippe Mourrain

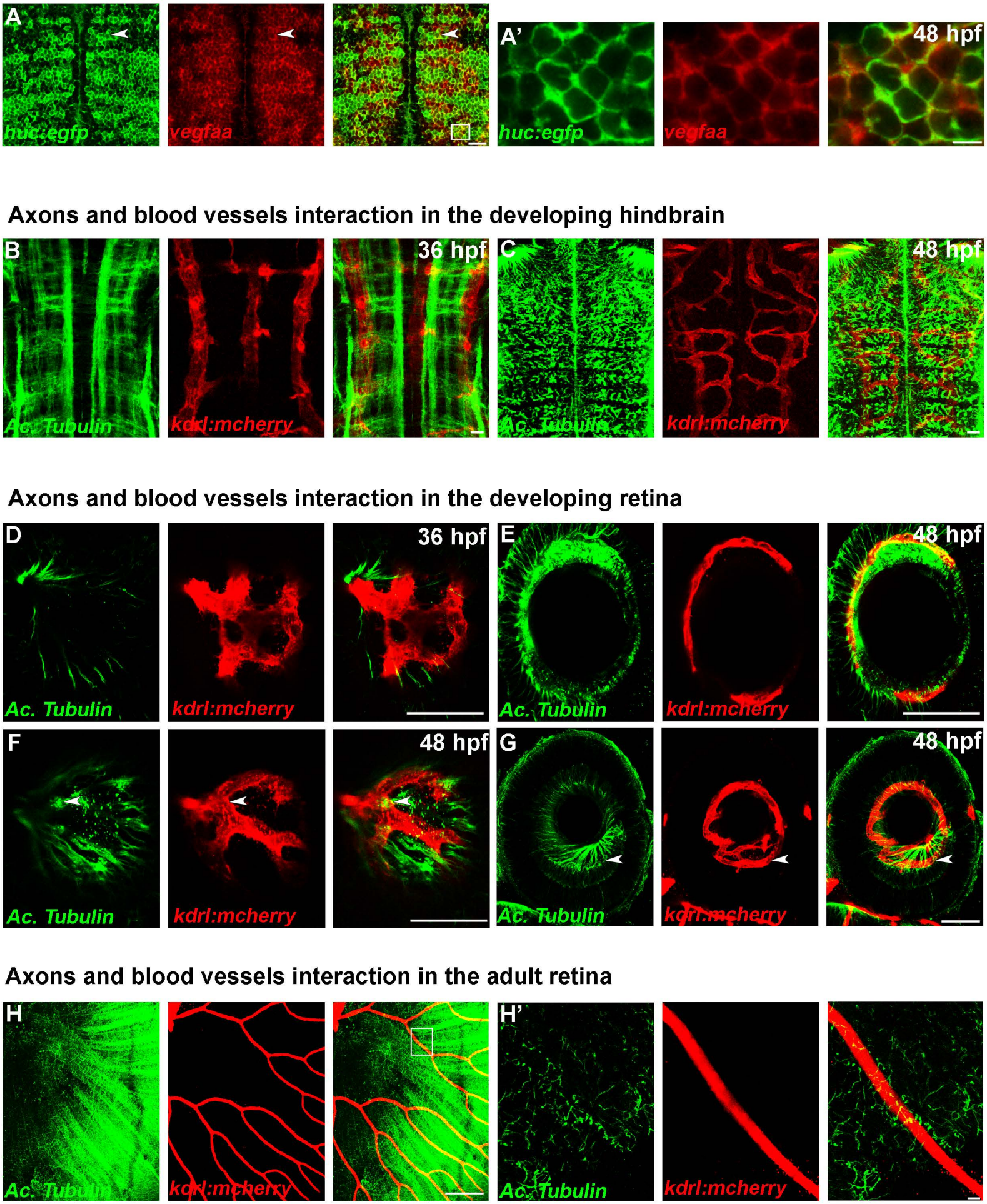
Zebrafish neuronal *vegfa* expression in the developing hindbrain
A
huc:egfp
vegfaa
A'
huc:egfp
vegfaa
48 hpf
Axons and blood vessels interaction in the developing hindbrain
B
Ac. Tubulin
kdrl:mcherry
36 hpf
C
Ac. Tubulin
kdrl:mcherry
48 hpf
Axons and blood vessels interaction in the developing retina
D
Ac. Tubulin
kdrl:mcherry
36 hpf
E
Ac. Tubulin
kdrl:mcherry
48 hpf
F
Ac. Tubulin
kdrl:mcherry
48 hpf
G
Ac. Tubulin
kdrl:mcherry
48 hpf
Axons and blood vessels interaction in the adult retina
H
Ac. Tubulin
kdrl:mcherry
H'
Ac. Tubulin
kdrl:mcherry

Figure S1

Supplemental Figure 1: Neurons expressing VEGF-A are closely associated with blood vessels (related to Figure 1)

(A) Confocal section of double *in situ*/immunolabelling with *vegfaa* and EGFP in the hindbrain of *Tg(huc:egfp)* line at 48 hpf shows neuronal expression of *vegfa* in the zebrafish brain. Close up of *vegfaa* expression in the hindbrain (A'). **(B, C)** Confocal section of double immunolabelling showing the physical interaction/close proximity between axons (Acetyl Tubulin, green) and blood vessels (red) in *Tg(kdrl:mCherry)* hindbrain at 36 and 48 hpf. **(D-H)** Confocal section of double immunolabelling showing the physical interaction/close proximity between axons (Acetyl Tubulin, green) and blood vessels (red) in *Tg(kdrl:mCherry)* retina at 36 hpf, 48 hpf or in the adult retina. Close up on a blood vessel in the adult retina (H'). Arrowheads show co-localization. Dorsal view of the brain with anterior up. Lateral view of the retina. Scale bars: 100 μm (A and D-H) or 10 μm (A', B, C and H').

A zebrafish NSCs
in the developing hindbrain

B zebrafish NSCs in the adult
ventricular zone of the telencephalon

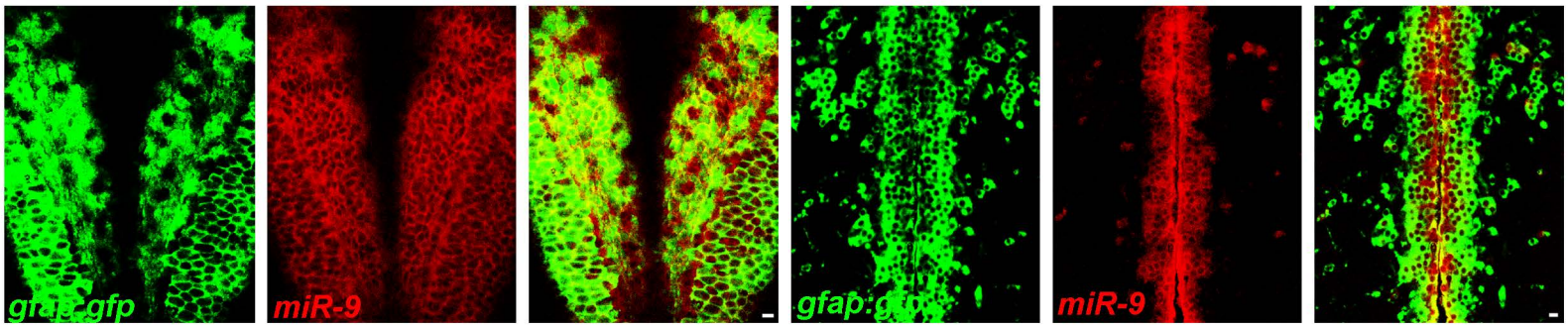

C Dynamic of *miR-9* expression during development

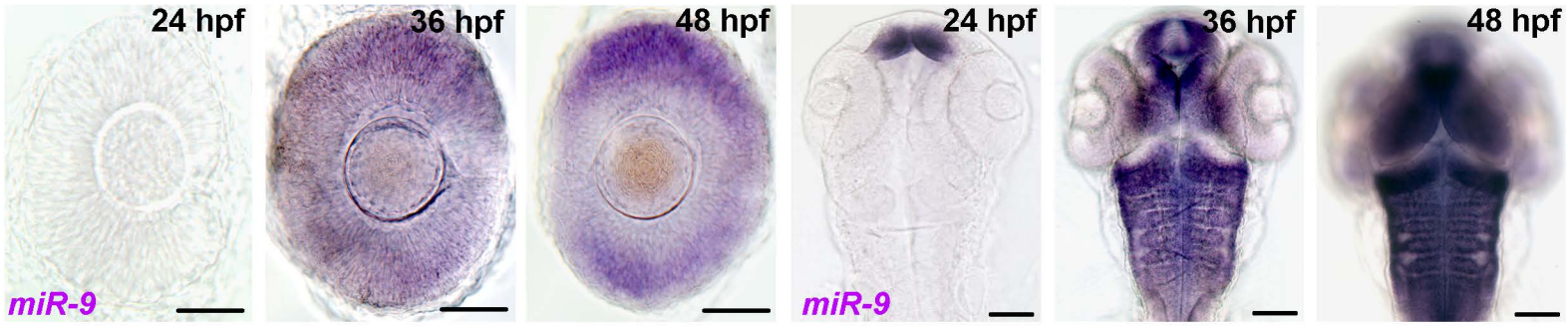

Figure S2

Supplemental Figure 2: miR-9 expression in NSCs in the zebrafish brain (related to Figure 1)

(A, B) Confocal section of double in situ/immunolabelling showing extensive overlap in the expression of endogenous *miR-9* and EGFP protein in hindbrain at 72 hpf or in the ventricular zone of the adult zebrafish telencephalon in the *Tg(gfap:gal4)*, *Tg(uas:egfp)* line, revealing miR-9 expression in embryonic and adult NSCs. **(C)** Whole-mount in situ hybridization against *miR-9* showing the time course of *miR-9* expression in the developing embryo at 24, 36 and 48 hpf. Dorsal view of the brain with anterior up. Lateral view of the retina. Scale bars: 10 μm (A, B) or 100 μm (C).

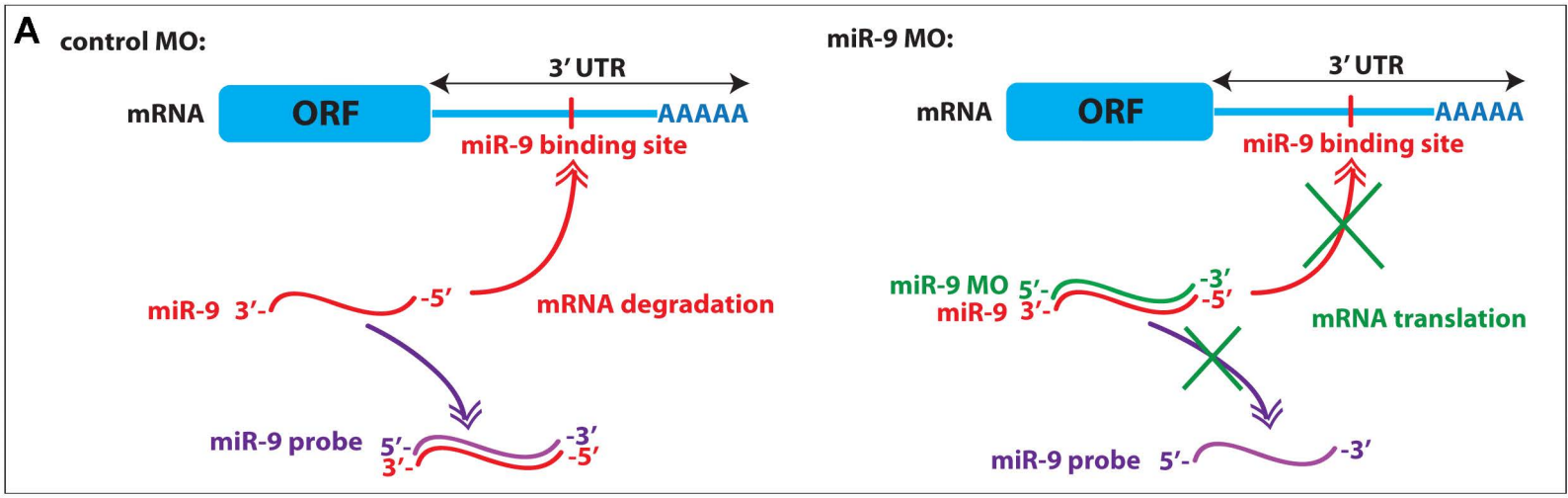
A
control MO:
mRNA
ORF
3′ UTR
AAAAA
miR-9 binding site
miR-9 3′-
-5′
mRNA degradation
miR-9 probe
5′-
3′-
-3′
-5′
miR-9 MO:
miR-9 MO 5′-
miR-9 3′-
-3′
-5′
mRNA translation
miR-9 probe 5′-
-3′

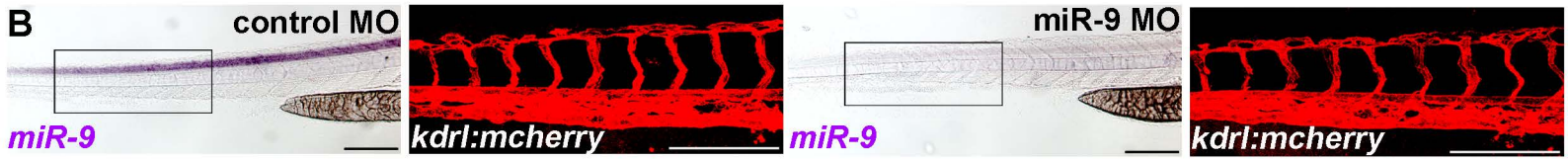
B
control MO
miR-9
kdrl:mcherry
miR-9 MO
miR-9
kdrl:mcherry


C
control MO
Box1
Box2
miR-9 MO
Box1
Hyloid vasculature
Box3

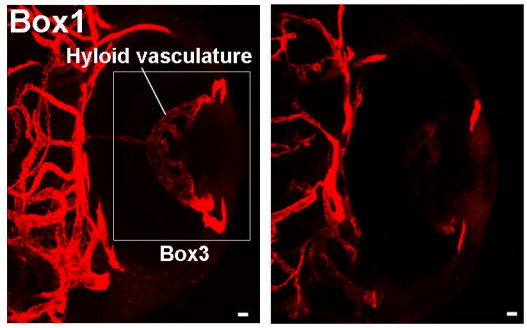
Box3
kdrl:mcherry

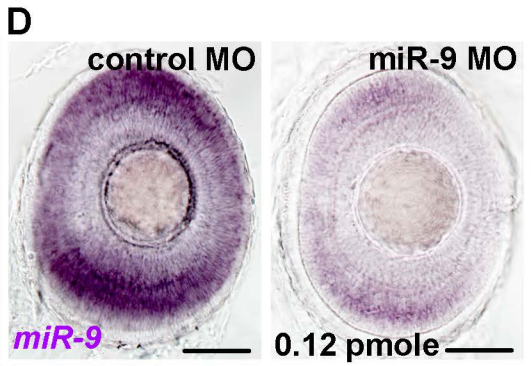
D
control MO
miR-9
miR-9 MO
0.12 pmole
miR-9 MO
0.5 pmole
miR-9 MO
2 pmole


group 1
group 2
group 3
group 4
kdrl:mcherry

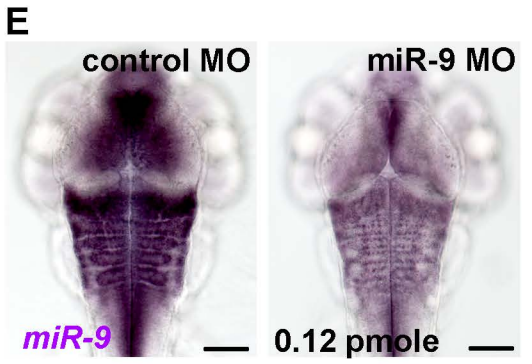
E
control MO
miR-9
miR-9 MO
0.12 pmole
miR-9 MO
0.5 pmole
miR-9 MO
2 pmole

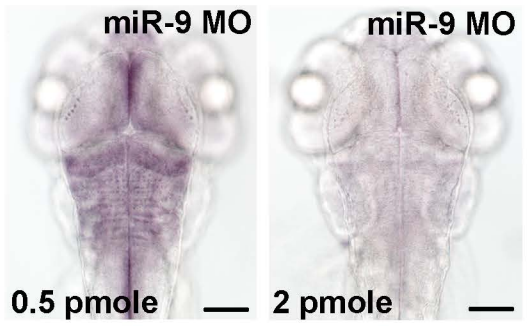
Box2
PCS
PHBC
CtA
BA
control MO
miR-9 MO
0.12 pmole
miR-9 MO
0.5 pmole
miR-9 MO
2 pmole

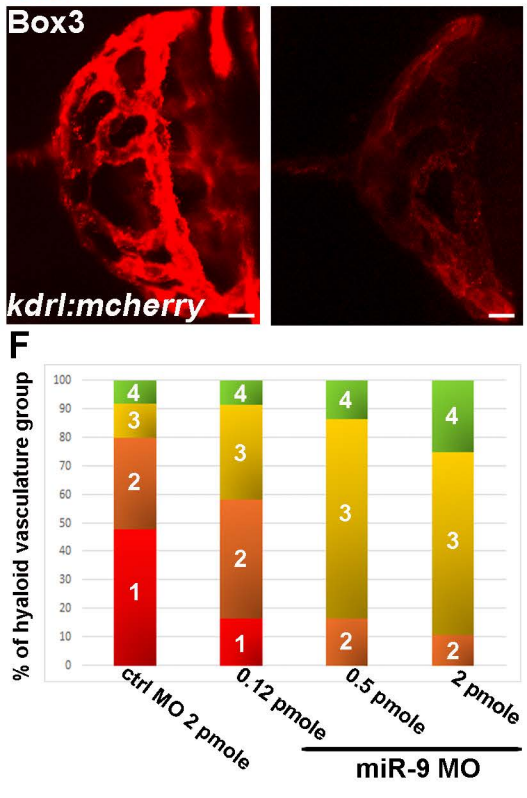
F
% of hyaloid vasculature group
100
90
80
70
60
50
40
30
20
10
0
ctrl MO 2 pmole
0.12 pmole
0.5 pmole
2 pmole
miR-9 MO

Figure S3

Supplemental Figure 3: miR-9 controls the neurovasculature formation in a dose dependent manner (related to Figure 2)

(A) Schematic representation of the miR-9 MO binding to microRNA-9. With the control MO, miR-9 is available, allowing the degradation of the mRNA target and revealing the *miR-9* expression pattern with the specific miR-9 LNA probe. In presence of the miR-9 MO, miR-9 is bound by the MO, inhibiting the mRNA degradation and the binding of the LNA probe. **(B)** Whole-mount in situ hybridization against miR-9 at 72 hpf shows that miR-9 knockdown does not affect trunk morphogenesis.mCherry immunolabelling in *Tg(kdrl:mCherry)* at 72 hpf showing blood vessels formation in the trunk of control or miR-9 morphant larvae. In the trunk, miR-9 knockdown does not affect blood vessels development. **(C)** Confocal projections of mCherry immunolabelling in *Tg(kdrl:mCherry)* at 72 hpf showing blood vessels formation in control or miR-9 morphant larvae in the brain. The affected neurovasculature in the midbrain, hindbrain and retina is highlighted by an asterisk. (**D, E**) Whole-mount in situ hybridization against *miR-9* at 72 hpf in larvae injected with the control MO or the miR-9 MO in the retina (D) and brain (E). Confocal projections of mCherry immunolabelling in *Tg(kdrl:mCherry)* at 72 hpf showing blood vessels formation in control MO and miR-9 MO injected larvae. Higher is the quantity of miR-9 MO injected in the egg, stronger is inhibition of *miR-9* expression. The severity of the neurovasculature defects is correlated to the level of miR-9 inhibition. (**F**) The formation of the hyaloid vasculature in the retina of control MO (n=25) or miR-9 MO dilution series (n=24, 30 and 28 for croissant dilutions respectively) at 72 hpf was classified in four groups and quantified. Group 1: The blood vessels form a complex vascular network. Group 2: The hyaloid vasculature shows a reduced branching complexity. Group 3: In addition to the reduction of the branching, the caliber is affected and some vessels appear to be thicker. Group 4: The hyaloid vasculature is absent. Dorsal view of the brain with anterior up. Lateral view of the retina. Box1 is a close up of the retina. Box2 is a close up of the hindbrain. Box3 is a close up of the hyaloid vasculature in the retina. Scale bars: 10 µm for immunolabelling and 100 µm for whole mount ISH.

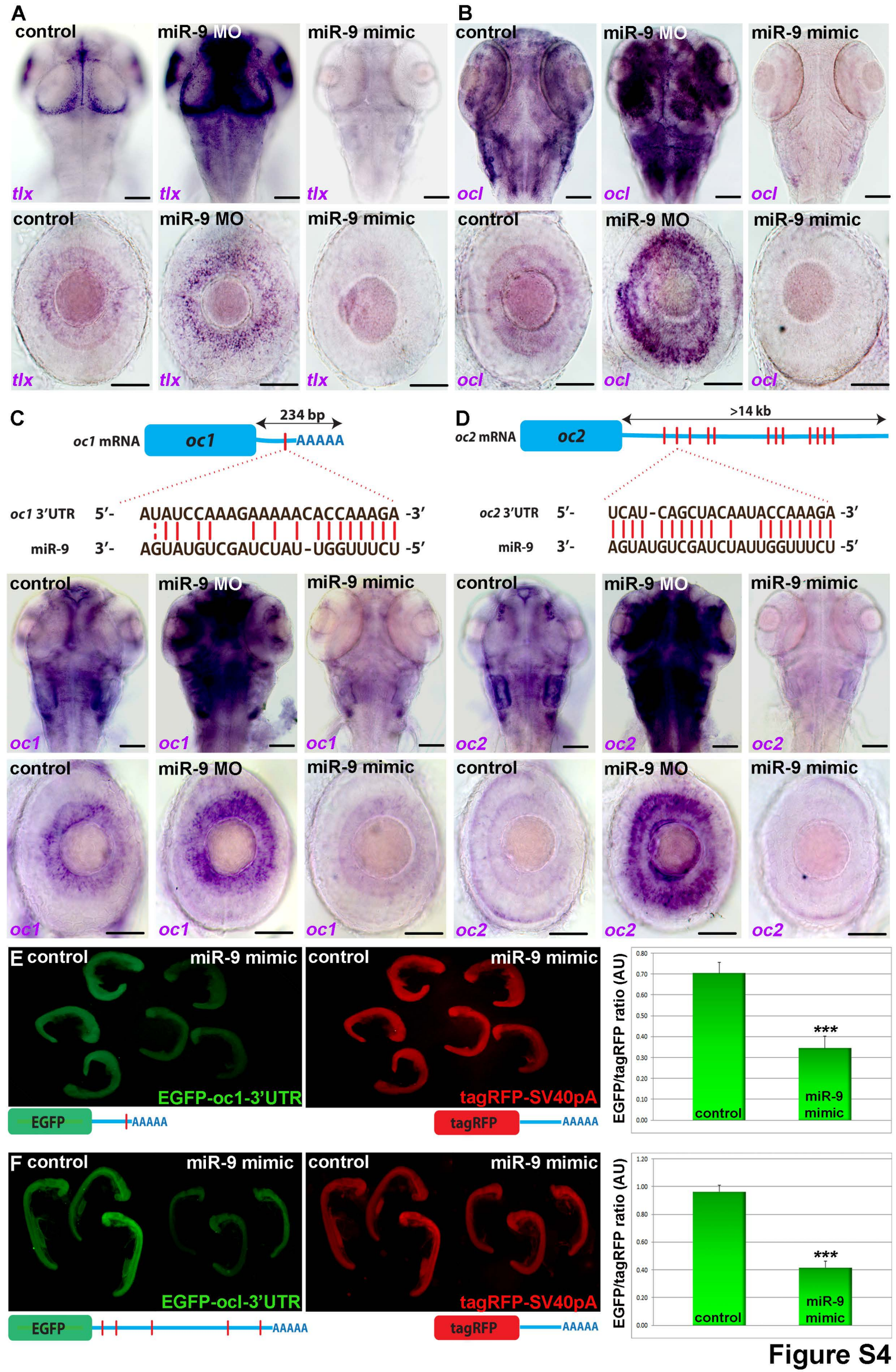
A
control
miR-9 MO
miR-9 mimic
tlx
B
ocl
C
234 bp
oc1 mRNA
oc1
AAAAA
oc1 3'UTR 5'- AUAUCCAAAGAAAAACACCAAAGA -3'
miR-9 3'- AGUAUGUCGAUCUAU-UGGUUUCU -5'
D
>14 kb
oc2 mRNA
oc2
oc2 3'UTR 5'- UCAU-CAGCUACAAUACCAAAGA -3'
miR-9 3'- AGUAUGUCGAUCUAUUGGUUUCU -5'
oc1
oc2
E control
miR-9 mimic
EGFP-oc1-3'UTR
tagRFP-SV40pA
EGFP
tagRFP
AAAAA
EGFP/tagRFP ratio (AU)
***
F
EGFP-ocl-3'UTR

Figure S4

Supplemental Figure 4: Validation of miR-9 targets conserved across vertebrates (related to Figure 3)

(A, B) Whole-mount in situ hybridization against *tlx* (A) or *ocl* (B) in larvae at 72 hpf injected with the control MO, the miR-9 MO or the miR-9 RNA mimic. *tlx* and *ocl* behave like a miR-9 target showing an increase in the miR-9 knockdown and a decrease in the miR-9 gain of function. **(C, D)** Schematic representation of the zebrafish *oc1* (C) and *oc2* (D) mRNA indicating the sequence of the putative miR-9 binding sites in the 3'UTR (red). Whole-mount in situ hybridization against *oc1* (C) and *oc2* (D) in larvae at 72 hpf injected with the control MO, the miR-9 MO or the miR-9 RNA mimic. *onecut* family mRNAs behave like miR-9 targets showing an increase in the miR-9 knockdown and a decrease in the miR-9 gain of function. (**E, F**) Fluorescent sensor assay to test the functionality of miR-9 binding sites in the 3'UTR of *oc1* (E) and *ocl* (F) showing that miR-9 mediates *oc1* and *ocl* inhibition via the 3'UTR. TagRFP and EGFP protein expression in embryos at 24 hpf: embryos were co-injected with the *egfp* mRNA containing the 3'UTR of *oc1* (n=7) or *ocl* (n=3) fused to the SV40pA and the internal control, *tagrfp* mRNA (n=8 and 3 respectively) in the presence or absence of miR-9 mimic. The ratio between the level of EGFP and TagRFP proteins fluorescence shows a decrease in EGFP expression, but not TagRFP, in the presence of the miR-9 RNA mimic. Dorsal view of the brain with anterior up. Lateral view of the retina. Scale bars: 100 μm. Error bars represent s.d. **P*<0.05, ***P*<0.001, ****P*<0.0005, determined by *t*-test, two-tailed.

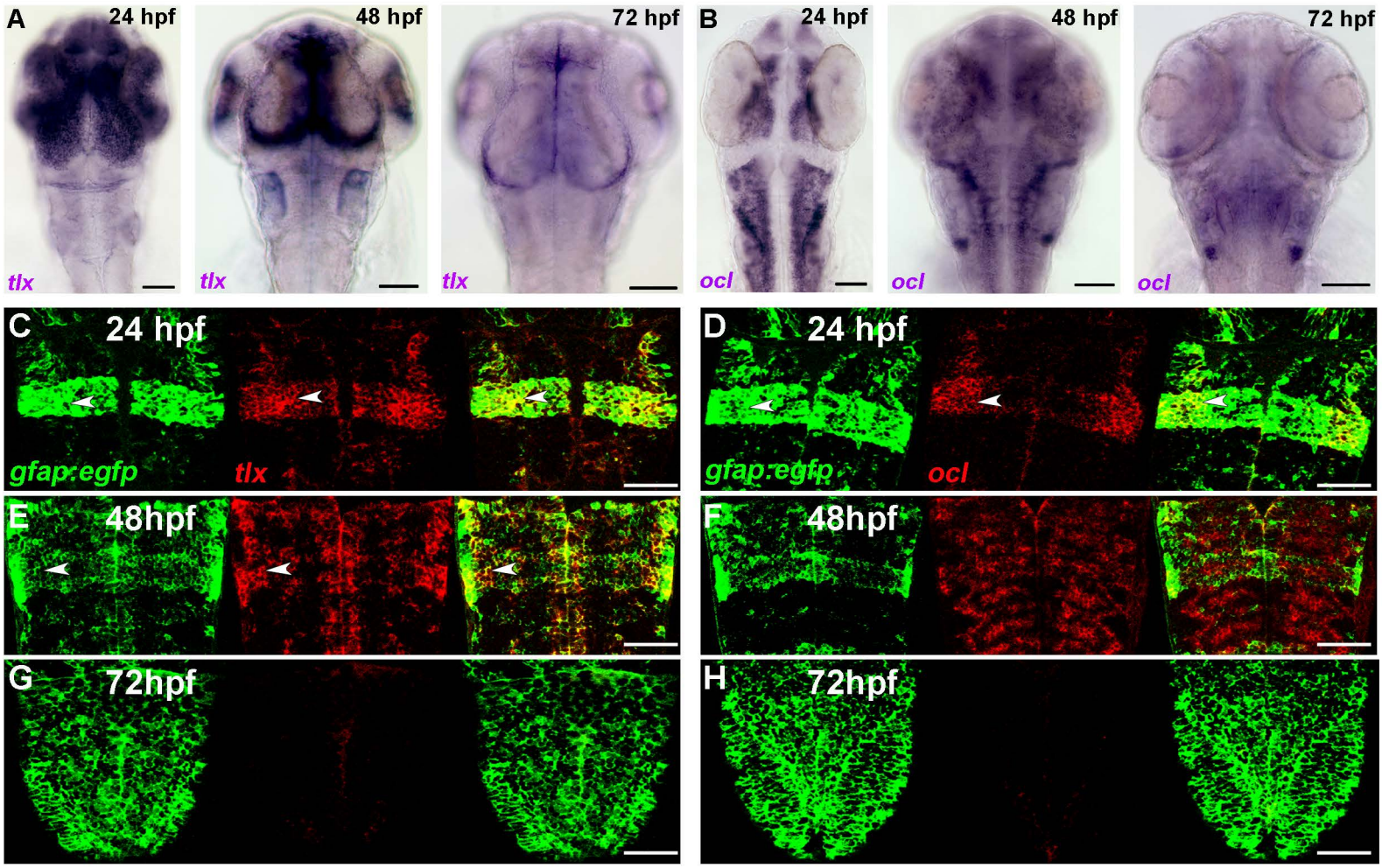
A
24 hpf
48 hpf
72 hpf
tlx
tlx
tlx
B
24 hpf
48 hpf
72 hpf
ocl
ocl
ocl
C
24 hpf
gfap:egfp
tlx
D
24 hpf
gfap:egfp
ocl
E
48hpf
F
48hpf
G
72hpf
H
72hpf

Figure S5

Supplemental Figure 5: Neural expression of *tlx* and *ocl* (related to Figure 3)

(A, B) Whole-mount in situ hybridization showing the time course of *tlx* (A) and *ocl* (B) expression in the developing embryo at 24, 48 and 72 hpf. During development, when *miR-9* expression becomes broader and stronger after 24 hpf, we observe a correlative decrease in *tlx* and *ocl* expression. (**C-H**) Confocal section of double in situ/immunolabelling with *tlx* or *ocl* mRNAs and EGFP in the *Tg(gfap:gal4); Tg(uas:egfp)* line labelling NSCs in the hindbrain. When miR-9 is not expressed broadly throughout the brain at 24 hpf, we observed an overlap in the expression of *tlx* and *ocl* with the NSCs marker GFAP (C, D). At 48 hpf, when miR-9 is strongly expressed in the brain *ocl* is excluded from the NSCs domain (E, F). At 72 hpf, both *tlx* and *ocl* are not detected in NSCs (G, H). Arrowheads show co-localization with EGFP. Dorsal view of the brain with anterior up. Scale bars: 100 µm.

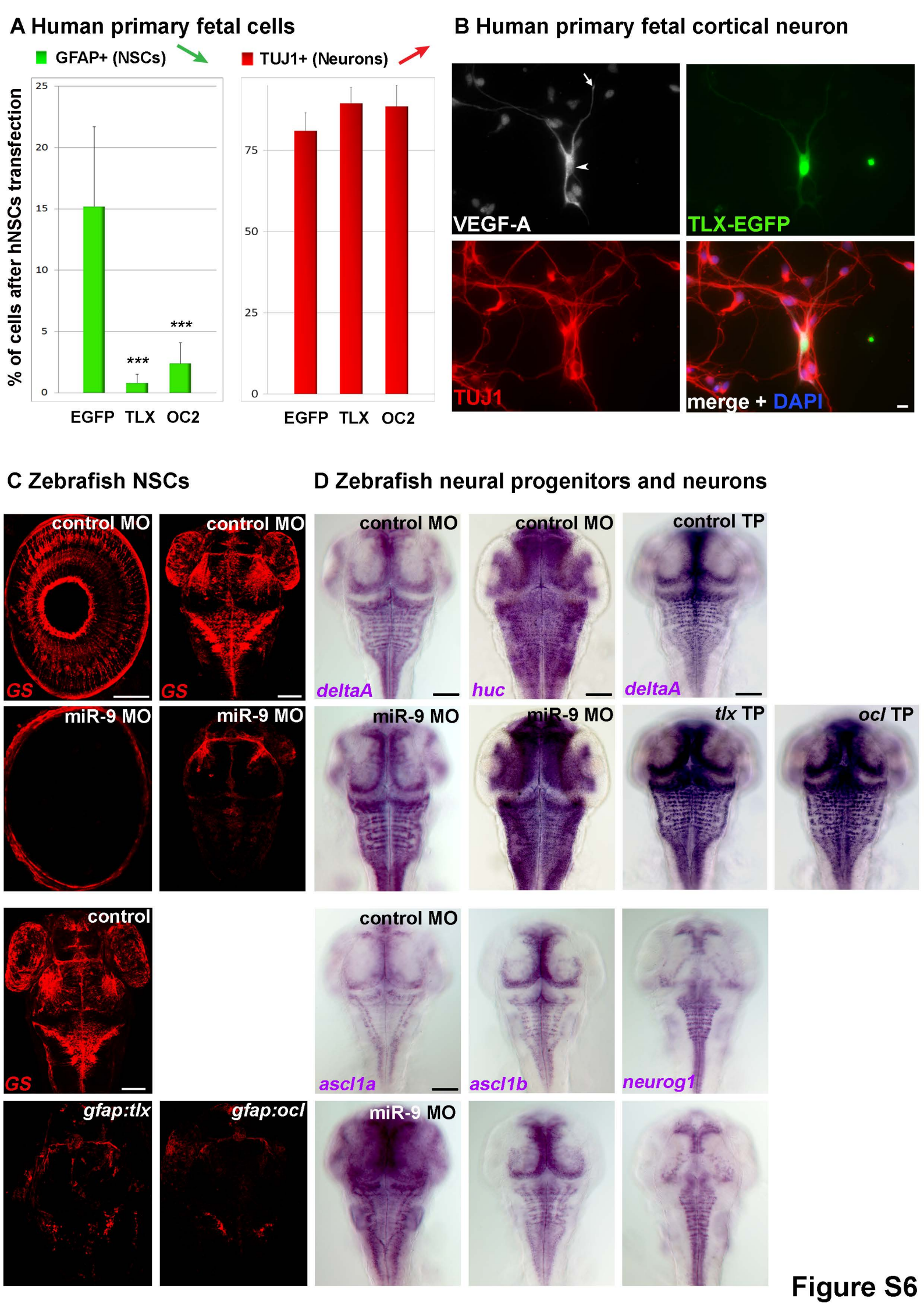
A Human primary fetal cells
GFAP+ (NSCs)
TUJ1+ (Neurons)
% of cells after hNSCs transfection
25
20
15
10
5
0
***
***
EGFP TLX OC2
75
50
25
0
EGFP TLX OC2
B Human primary fetal cortical neuron
VEGF-A
TLX-EGFP
TUJ1
merge + DAPI
C Zebrafish NSCs
control MO
control MO
GS
GS
miR-9 MO
miR-9 MO
control
GS
gfap:tlx
gfap:ocl
D Zebrafish neural progenitors and neurons
control MO
control MO
control TP
deltaA
huc
deltaA
miR-9 MO
miR-9 MO
tlx TP
ocl TP
control MO
ascl1a
ascl1b
neurog1
miR-9 MO

Figure S6

Supplemental Figure 6: TLX and OC activity control neural stem cells fate (related to Figure 4)

(A) *In vitro* effect of transfecting primary human embryonic neural stem cells with a control EGFP plasmid, TLX-p2A-EGFP or OC2-p2A-EGFP. Overexpression of TLX (n=646) and OC2 (n=528) significantly depletes the existing neural stem cell population in the dish compared to the EGFP control (n=408). Furthermore, in comparison with EGFP transfection (n=344), expression of TLX (n=99) and OC2 (n=69) slightly increases the percentage of primary human NSCs that differentiate into cortical neurons. **(B)** Triple immunolabelling against TUJ1, EGFP and VEGF-A after transfection of primary human embryonic NSCs with the TLX-p2A-EGFP plasmid (nuclear marker DAPI is in blue). Embryonic cortical neuron express high detectable level of nuclear (arrowhead) and cytoplasmic (arrow) VEGF-A after TLX expression (EGFP). **(C)** Confocal projection of immunolabelling with endogenous GS protein in the brain of control MO or miR-9 MO injected larvae and larvae expressing *uas:tlx* or *uas:ocl* in NSCs using *Tg(gfap:gal4)* line at 72 hpf. Embryonic NSCs are reduced in the miR-9 depleted and *tlx* or *ocl* expressing brain. **(D)** Whole-mount in situ hybridization against *deltaA*, *ascl1a*, a*scl1b*, *neurog1* or *huc* in embryos at 48 hpf injected with the control MO, miR-9 MO*, tlx* TP or *ocl* TP. miR-9 inhibition increases neural progenitor cells (*deltaA* and *ascl1a*) and promote a neuronal fate (*huc*). *tlx* or *ocl* mRNA protection also leads to an increase in *deltaA*+ neural progenitors in the zebrafish brain. Of note, miR-9 morphant shows an increase in *deltaA*+ and *ascl1a*+ NPCs but not *ascl1b*+ or *neurog*1+ NPCs. Dorsal view, Anterior up. Scale bars: 10 µm (B) or 100 µm (C, D). Error bars represent s.d. **P*<0.05, ***P*<0.001, ****P*<0.0005, determined by *t*-test, two-tailed.

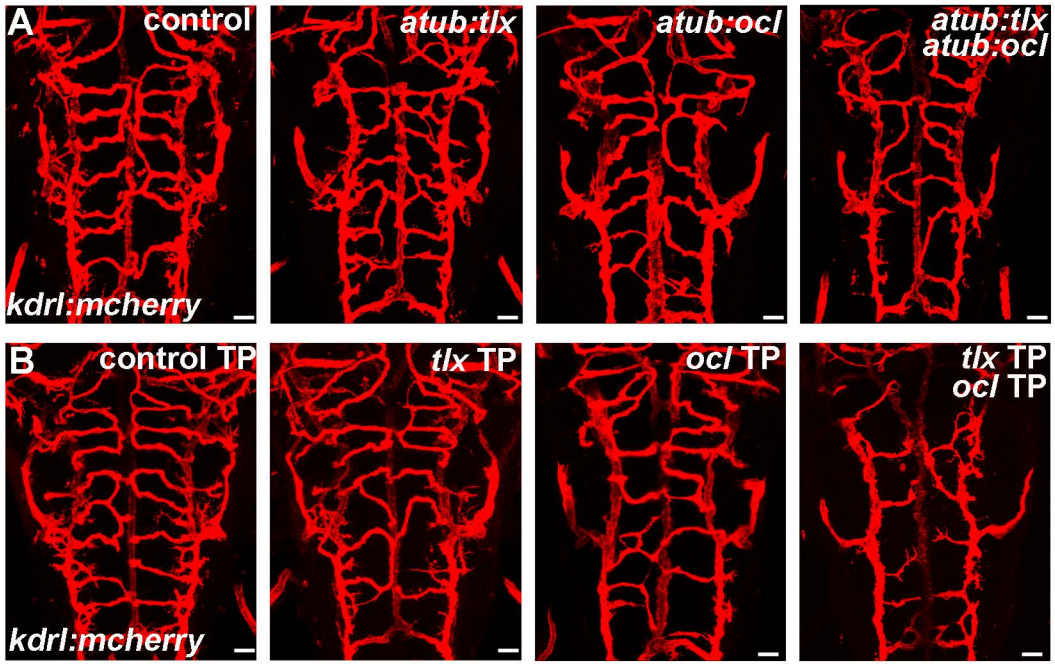
A
control
atub:tlx
atub:ocl
atub:tlx
atub:ocl
kdrl:mcherry
B
control TP
tlx TP
ocl TP
tlx TP
ocl TP
kdrl:mcherry

Figure S7

Supplemental Figure 7: Tlx and Ocl neuronal expression affect vasculature development (related to Figure 4)

(A) Confocal projections of mCherry immunolabelling in *Tg(kdrl:mCherry)* at 72 hpf showing blood vessels formation in the hindbrain of controls or larvae expressing *uas:tlx*, *uas:ocl* or *uas:tlx* and *uas:ocl* in a pan-neuronal manner in *Tg(alpha-tubulin:gal4)* line. **(B)** Confocal projections of mCherry immunolabelling in *Tg(kdrl:mCherry)* at 72 hpf showing blood vessels formation in the hindbrain of control MO, *tlx* TP, *ocl* TP or *tlx* and *ocl* TP larvae**.** Dorsal view of the brain with anterior up. Scale bars: 10 µm.

SUPPLEMENTAL EXPERIMENTAL PROCEDURES

Primary human embryonic neural stem cells culture, purification and transfection

Human fetal cortex was collected after elective abortion by a commercial vendor (StemExpress, Placervill, CA). The meninges were removed and the tissue was enzymatically dissociated to make a suspension of single cells as described previously (Cahoy et al., 2008; Dugas et al., 2006). Briefly, the tissue was incubated at 33°C for 45 minutes in 20 ml of a papain solution containing Earle's balanced salts (EBSS, Sigma, St. Louis, MO, E7510), D(+)-glucose (22.5mM), NaHCO3 (26mM), DNase (125U/ml, Worthington, Lakewood, NJ, LS002007), papain (4 U/ml, Worthington, Lakewood, NJ, LS03126), and L-cysteine (1mM, Sigma, St. Louis, MO, C7880). The papain solution was equilibrated with 5% CO2 and 95% O2 gas before and during papain treatment. Following papain treatment, the tissue was washed three times with 4.5ml of inhibitor buffer containing BSA (1.0mg/ml, Sigma, St. Louis, MO, A-8806), and ovomucoid (also known as trypsin inhibitor, 1.0 mg/ml, Roche Diagnostics Corporation, Indianapolis, IN 109878) and then mechanically dissociated by gentle sequential trituration using a 5ml pipette. Dissociated cells were layered on top of 10ml of high concentration inhibitor solution with 5mg/ml BSA and 5mg/ml ovomucoid and centrifuged at 130g for 5 minutes. The cell pellet was then resuspended in 12 ml Dulbecco's phosphate-buffered saline (DPBS, Invitrogen, Carlsbad, CA 14287) containing 0.02% BSA and 12.5U/ml DNase and filtered through a 20um Nitex mesh (Sefar America Inc., Depew NY, Lab Pak 03-20/14) to remove undissociated cell clumps. Cell health was assessed by trypan blue exclusion.

To purify neural stem cells, the single cell suspension was immunopanned with a CD15 antibody (BD, mouse) for a 30 minute incubation. The adherent cells on the CD15 plate were washed 8 times with 10-20 ml of DPBS to remove all antigen-negative nonadherent cells, and then removed from the plate by treating with trypsin (Sigma, 1,000U/ml, T-4665) in 8ml Ca^{2+} and Mg^{2+} free EBSS (Irvine Scientific, Santa Ana, CA, 9208) for 3-10 minutes at 37°C in a 10% CO2 incubator. The cells were dislodged by gentle squirting of over the plate and harvested by centrifugation at 200g for 10 minutes.

Plasmid transfection was performed on purified neural stem cells from 14 week-old human fetal brains. TLX and ONECUT2 ORF were amplified by PCR from human cDNA, fused to the p2A-EGFP and cloned in the pCDNA3.1 vector downstream of a CMV promoter. EGFP, TLX, and OC2 plasmids were transfected into cells using the nucleofector kit (Lonza) for primary neural stem cells. 2-4ug of each plasmid was added to the cell suspension and briefly electoporated according to the user protocol. Cells were then plated on PDL coated coverslips and cultured in a defined media including DMEM, insulin, pyruvate, Pen/Strep, L-glutamine, Sato, and N-acetylcysteine. Two 14 week-old brains were used to prepare 6 samples for each condition, each sample containing 150-450 cells.

Generation of human iPSC-derived cortical neurons

Human iPSCs derived from healthy individuals were grown on inactivated mouse embryonic fibroblasts feeders in iPSC medium (DMEM/F12, 20% Knockout Serum, 1mM non-essential amino acids, GlutaMax (1:200),

0.1mM β-mercaptoethanol, penicillin and streptomycin (1:100)). Colonies of iPSCs were detached with dispase (0.35mg/ml, Invitrogen) and transferred into low-attachment plates in iPSC medium supplemented with dorsomorphin (5 µM, Sigma) and SB-431542 (10 µM, Tocris), and the medium was changed daily. On day six of *in vitro* differentiation, neural spheroids were transferred to neural medium (NM) (Neurobasal A, B27 without vitamin A, GlutaMax (1:100), penicillin and streptomycin (1:100); Life Technologies), which was supplemented with EGF (20 ng/ml) and FGF2 (20 ng/ml) until day 24, and then supplemented with BDNF (20 ng/ml) and NT3 (20 ng/ml) from day 25 to 42. From day 43 onwards, cortical spheroids were maintained in NPC with medium changes every 4 days.

For enzymatic dissociation and culture in monolayer (Deverman et al., 2016), hCS were incubated with accutase for 15 minutes at 37°C, washed 3 times with NM and gently triturated with a P-200 pipet. Cells were plated on poly-ornithine and laminin coated glass coverslips (15 mm) at around 300,000 cells/well and maintained in NM supplemented with BDNF (20 ng/ml) and NT3 (20 ng/ml) with half medium changes every other day.

Zebrafish transgenic lines and plasmid construction

The following transgenic lines were used to visualize: post-mitotic neurons *Tg(huc:egfp)* (Park et al., 2000), neural stem cells *Tg(gfap:gal4); Tg(uas:egfp), miR-9* expressing cells *Tg(CNE1:egfp),* referred as *Tg(hsa-MIR-9-2:egfp)* or endothelial cells *Tg(kdrl:ras-mCherry*) (Chi et al., 2008) and *Tg(kdrl:egfp*) (Choi et al., 2007a).

For the generation of *Tg(alpha-tubulin:gal4)* and *Tg(gfap:gal4)*, the goldfish *a1-tubulin* promoter (Hieber et al., 1998) and the zebrafish *gfap* promoter (Bernardos and Raymond, 2006) were cloned into the p5E 5' entry vector of the tol2kit (Kwan et al., 2007). Then, the 5' entry vector was recombined into the Tol2 transposon destination vector. *pTol2-vegfaa:egfp* was by made by PCR amplification of 1.5kb upstream of the *vegfaa* promoter from zebrafish genomic DNA. PCR products were directionally cloned into the XhoI and BglII sites of the pTol2-E1b:EGFP vector. To establish *Tg(alpha-tubulin:gal4), Tg(gfap:gal4) and Tg(*CNE1*:egfp)* stable transgenic lines, plasmids were injected into one-cell stage embryos with the Tol2 mRNA transposase (Kwan et al., 2007).

To generate *pDestTol2-uas:vegfaa*, *pDestTol2-uas:tlx*, *pDestTol2-uas:ocl*, *pDestTol2-uas:tlx-p2A-egfp*, *pDestTol2-uas:ocl-p2a-egfp pDestTol2-hs:tlx*, *pDestTol2-hs:ocl*, *pDestTol2-hs:tlx-p2A-egfp* and *pDestTol2-hs:ocl-p2A-egfp* plasmids for transient expression; *vegfaa*, *tlx* and *ocl* ORF were amplified by PCR from zebrafish cDNA and cloned in the pME entry vector of the tol2kit. The appropriate middle entry clone was mixed with the UAS or the heat-shock promoter 5' entry vector and the SV40pA 3' entry vector, and recombined into the Tol2 transposon destination vector (Kwan et al., 2007).

I*n situ* hybridization

In situ hybridizations were performed as previously described (Oxtoby and Jowett, 1993). Previously described antisense DIG labelled probes for *neurog1* (Blader et al., 1997), *deltaA* (Haddon et al., 1998), *ascl1a* and *ascl1b* (Allende and Weinberg, 1994) were generated using standard procedures. ORFs were cloned in a pCS2+ vector using zebrafish cDNA for *vegfaa, tlx, oc1, oc2,* and *ocl* or human cDNA for *SOX2*; and antisense DIG

labelled probes were transcribed using the linearized pCS2+ plasmid containing the ORF. For miR-9 ISH, the previously described miRCURY detection probe (LNA) hsa–miR-9 (Exiqon) was used (Leucht et al., 2008). *In situs* were revealed using either BCIP and NBT (Roche) or Fast Red (Roche) as substrates.

Antisense morpholino and microRNA-9 mimic injection

We used the previously described miR-9 MO (TCATACAGCTAGATAACCAAAGA) and the control MO (CACCAAACCATATAGAAGTGATA) (Leucht et al., 2008). Embryos were injected at the one-cell stage with 0.12 to 2 pmole of the miR-9 or control MO. *tlx* (GCTTGCTCATATTGAAGACCACGGC) and *ocl* (ACATCTCTCCCATATTACCATCCAT) MOs were injected at 1 pmole and the efficiency of the MO was tested by the capacity of the MO to down-regulate EGFP (but not the internal mCherry control) expression driven by a construct containing the MO binding site in the 5'UTR of *tlx* or *ocl* fused to a p2A-EGFP (data not shown). For target protection, *tlx* TP (CCTTTGGTTTTCAGCACTATGTCAA), *ocl* TP (TCTTTGGTATTGGGACTCCTATCAG), and control TP (CTGTGGCCTAAAGGGTCTAGACATG) were designed as previously described (Choi et al., 2007b; Staton and Giraldez, 2011) and used at 1 pmole.

Gain of function of miR-9 was performed with the injection of the *mirVana* miR-9 RNA mimic, hsa-miR-9-5 (2 µM, Ambion).

Mosaic analysis

For mosaic expression of *uas:vegfaa*, *uas:tlx*, *uas:ocl*, *uas:tlx-p2A-egfp*, *uas:ocl-p2A-egfp*, *hs:tlx*, *hs:ocl*, *hs:tlx-p2A-egfp* and *hs:ocl-p2A-egfp,* the appropriate Tol2 based construct (25 ng/µl) was co-injected with synthetic mRNA encoding the Tol2 transposase (25ng/µl) into one-cell stage embryos. Heat-shocks were performed in a water bath at 37°C for 1 hour. For pan-neuronal expression using the *uas* promoter, the injection was performed in embryos from crosses between identified heterozygote carriers of *Tg(alpha-tubulin:gal4)* and *Tg(kdrl:ras-mCherry)*. Expression in neural stem cells was performed by injection in the *Tg(gfap:gal4)* line.

Drug treatments

Tg(*kdrl:ras-mCherry*) embryos were treated with 0.06 µM solution of the chemical tyrosine kinase inhibitor SU5416 (S8442, Sigma Aldrich) dissolved in DMSO (Herbert et al., 2009). Treatments started at 30 hpf and both DMSO and SU5416 treated embyos were fixed at 72 hpf to quantify the blood vessels sprouting.

Fluorescent sensor assay

Fluorescent sensor assay with the 3'UTR of *oc1* and *ocl* was performed as described in (Staton and Giraldez, 2011). Capped mRNAs for EGFP containing the *oc1* or *ocl* 3'UTR and TagRFP reporter constructs were synthetized using linearized pCS2+ plasmids and mMessage mMachine kit (Ambion). Zebrafish embryos were injected at a one-cell stage with 150ng/µL of EGFP and TagRFP mRNAs and either a control or miR-9 RNA mimics (2 µM, Ambion). The ratio of EGFP/TagRFP fluorescence was quantified using ImageJ software.

In silico predictions

Putative targets for miR-9 in human were first searched using the ElMMo miRNA target prediction server (http://www.mirz.unibas.ch/ElMMo3). 3'UTR of orthologous genes in zebrafish were retrieved from the Ensembl web server and searched for conserved miR-9 binding sites (Bartel, 2009).

The miR-9 consensus binding sequence (Leucht et al., 2008) was queried against the 3'UTR of each human gene in the GRCh37 human reference (hg19) using LASTZ (version 1.02.00) with sensitive parameters (--hspthresh=500 --gappedthresh=500 --seed=match6). The highest scoring alignments from LASTZ were inspected for conservation using the UCSC 46-way multiple alignment (Karolchik et al., 2014).

SUPPLEMENTAL REFERENCES

Allende, M.L., and Weinberg, E.S. (1994). The expression pattern of two zebrafish achaete-scute homolog (ash) genes is altered in the embryonic brain of the cyclops mutant. Developmental biology *166*, 509-530.

Bartel, D.P. (2009). MicroRNAs: target recognition and regulatory functions. Cell *136*, 215-233.

Bernardos, R.L., and Raymond, P.A. (2006). GFAP transgenic zebrafish. Gene expression patterns : GEP *6*, 1007-1013.

Blader, P., Fischer, N., Gradwohl, G., Guillemot, F., and Strahle, U. (1997). The activity of neurogenin1 is controlled by local cues in the zebrafish embryo. Development *124*, 4557-4569.

Cahoy, J.D., Emery, B., Kaushal, A., Foo, L.C., Zamanian, J.L., Christopherson, K.S., Xing, Y., Lubischer, J.L., Krieg, P.A., Krupenko, S.A*., et al.* (2008). A transcriptome database for astrocytes, neurons, and oligodendrocytes: a new resource for understanding brain development and function. The Journal of neuroscience : the official journal of the Society for Neuroscience *28*, 264-278.

Chi, N.C., Shaw, R.M., De Val, S., Kang, G., Jan, L.Y., Black, B.L., and Stainier, D.Y. (2008). Foxn4 directly regulates tbx2b expression and atrioventricular canal formation. Genes & development *22*, 734-739.

Choi, J., Dong, L., Ahn, J., Dao, D., Hammerschmidt, M., and Chen, J.N. (2007a). FoxH1 negatively modulates flk1 gene expression and vascular formation in zebrafish. Developmental biology *304*, 735-744.

Choi, W.Y., Giraldez, A.J., and Schier, A.F. (2007b). Target protectors reveal dampening and balancing of Nodal agonist and antagonist by miR-430. Science *318*, 271-274.

Deverman, B.E., Pravdo, P.L., Simpson, B.P., Kumar, S.R., Chan, K.Y., Banerjee, A., Wu, W.L., Yang, B., Huber, N., Pasca, S.P*., et al.* (2016). Cre-dependent selection yields AAV variants for widespread gene transfer to the adult brain. Nature biotechnology *34*, 204-209.

Dugas, J.C., Tai, Y.C., Speed, T.P., Ngai, J., and Barres, B.A. (2006). Functional genomic analysis of oligodendrocyte differentiation. The Journal of neuroscience : the official journal of the Society for Neuroscience *26*, 10967-10983.

Haddon, C., Smithers, L., Schneider-Maunoury, S., Coche, T., Henrique, D., and Lewis, J. (1998). Multiple delta genes and lateral inhibition in zebrafish primary neurogenesis. Development *125*, 359-370.

Herbert, S.P., Huisken, J., Kim, T.N., Feldman, M.E., Houseman, B.T., Wang, R.A., Shokat, K.M., and Stainier, D.Y. (2009). Arterial-venous segregation by selective cell sprouting: an alternative mode of blood vessel formation. Science *326*, 294-298.

Hieber, V., Dai, X., Foreman, M., and Goldman, D. (1998). Induction of alpha1-tubulin gene expression during development and regeneration of the fish central nervous system. Journal of neurobiology *37*, 429-440.

Karolchik, D., Barber, G.P., Casper, J., Clawson, H., Cline, M.S., Diekhans, M., Dreszer, T.R., Fujita, P.A., Guruvadoo, L., Haeussler, M*., et al.* (2014). The UCSC Genome Browser database: 2014 update. Nucleic acids research *42*, D764-770.

Kwan, K.M., Fujimoto, E., Grabher, C., Mangum, B.D., Hardy, M.E., Campbell, D.S., Parant, J.M., Yost, H.J., Kanki, J.P., and Chien, C.B. (2007). The Tol2kit: a multisite gateway-based construction kit for Tol2 transposon transgenesis constructs. Developmental dynamics : an official publication of the American Association of Anatomists *236*, 3088-3099.

Leucht, C., Stigloher, C., Wizenmann, A., Klafke, R., Folchert, A., and Bally-Cuif, L. (2008). MicroRNA-9 directs late organizer activity of the midbrain-hindbrain boundary. Nature neuroscience *11*, 641-648.
Oxtoby, E., and Jowett, T. (1993). Cloning of the zebrafish krox-20 gene (krx-20) and its expression during hindbrain development. Nucleic acids research *21*, 1087-1095.
Park, H.C., Kim, C.H., Bae, Y.K., Yeo, S.Y., Kim, S.H., Hong, S.K., Shin, J., Yoo, K.W., Hibi, M., Hirano, T.*, et al.* (2000). Analysis of upstream elements in the HuC promoter leads to the establishment of transgenic zebrafish with fluorescent neurons. Developmental biology *227*, 279-293.
Staton, A.A., and Giraldez, A.J. (2011). Use of target protector morpholinos to analyze the physiological roles of specific miRNA-mRNA pairs in vivo. Nature protocols *6*, 2035-2049.